Quantifying Evapotranspiration in Seasonally Frozen Forests

A Thesis Submitted to the College of

Graduate and Postdoctoral Studies

In Partial Fulfillment of the Requirements

For the Degree of Master of Environment and Sustainability

In the School of Environment and Sustainability

University of Saskatchewan

Saskatoon

By

Sujan Basnet

Permission To use

In presenting this thesis in partial fulfillment of the requirements for a Postgraduate degree from the University of Saskatchewan, I agree that the Libraries of this University may make it freely available for inspection. I further agree that permission for copying of this thesis in any manner, in whole or in part, for scholarly purposes may be granted by the professor or professors who supervised my thesis work or, in their absence, by the Head of the Department or the Dean of the College in which my thesis work was done. It is understood that any copying or publication or use of this thesis or parts thereof for financial gain shall not be allowed without my written permission. It is also understood that due recognition shall be given to me and to the University of Saskatchewan in any scholarly use which may be made of any material in my thesis.

Disclaimer

Reference in this thesis to any specific commercial products, process, or service by trade name, trademark, manufacturer, or otherwise, does not constitute or imply its endorsement, recommendation, or favoring by the University of Saskatchewan. The views and opinions of the author expressed herein do not state or reflect those of the University of Saskatchewan and shall not be used for advertising or product endorsement purposes.

Requests for permission to copy or to make other uses of materials in this thesis in whole or part should be addressed to:

School of Environment and Sustainability

University of Saskatchewan

Room 323, Kirk Hall

117 Science Place

Saskatoon, Saskatchewan S7N 5C8, Canada

or

Dean

College of Graduate and Postdoctoral Studies

University of Saskatchewan

116 Thorvaldson Building,110 Science Place

Saskatoon, Saskatchewan S7N 5C9, Canada

Abstract

In seasonally frozen environments, hydrological processes are highly dynamic in the spring, during and following the melt period, and this is when most of the runoff and groundwater recharge happens. This is also when evapotranspiration (ET) fluxes start to increase in response to higher solar radiation and there is a resumption of photosynthesis in evergreen species. Root water uptake from frozen soils is poorly understood and may be poorly represented in Land Surface Models. Previous studies have shown that ET is overestimated in the Canadian Land Surface Scheme (CLASS) during the melt/thaw period. This thesis extends the work to look at three Boreal Ecosystem Research and Monitoring Sites (BERMS) in the boreal forest in Saskatchewan; Old Jack Pine, Old Black Spruce and Old Aspen. CLASS was used to simulate the energy and water balance of the vegetation, soil and snowpack at the three sites. A series of numerical experiments were undertaken to investigate in detail the controls on simulated fluxes within the CLASS model, and as a means to help us raise questions about how the real-world processes operate. The CLASS model does not represent the phenomenon of freezing point depression, and hence all freezing/thawing occurs at 0 ℃. The model predicted a significant amount of transpiration during the melt period while the soil is at 0 ℃ and ice is still present in the soil pores. It was hypothesized that plant water uptake should not occur from soil layers which contain ice, and would, in reality, be at temperatures below zero. Subtracting the transpiration that occurred from soil layers containing ice improved the simulated ET, compared with flux tower estimates. Therefore, it is suggested that implementing a freezing point depression in the model and including a water stress function to shut down transpiration when the soil temperature is ≤ 0 ℃ would improve the simulated evapotranspiration during the melt period. The study also showed that calibration of the model parameters improved the simulations but is unable to uniquely constrain the infiltration and soil drainage fluxes by either single objective (ET) or multi-objective (soil moisture and ET) calibration. Further research is needed to explore the physiology of trees and roots during the melt period.

Acknowledgement

These two years have allowed me to develop a passion for the field of hydrology. I am extremely fortunate to work with some of the best colleagues and advisors that I will forever remember.

To begin with, I am grateful to my supervisor, Dr. Andrew Ireson for providing me this opportunity along with support and guidance throughout my Master's degree. His patience, advice and suggestions are sincerely appreciated. I would also like to express my gratitude to my advisory committee members, Dr. Alan Barr and Dr. Colin Whitfield, for the feedback and suggestions throughout my research. I would also like to acknowledge Dr. Bruce Davison for accepting to undertake the role of being an external examiner.

I am indebted to my beloved parents for the love and support throughout my life. I would like to thank my colleagues Amankwah Seth Kwaku, Ines Sanchez Rodriguez, Rosa Brennan, Haley Brauner, Morgan Braaten and Menna Elrashidy for all the help with my research.

Finally, I wish to express my appreciation to all the people from School of Environment and Sustainability (SENS), Global Institute for Water Security (GIWS) and National Hydrology Research Centre (NHRC) for the facilities provided.

Table of Contents

LIST OF ABBREVIATION

AET	Actual rate of evapotranspiration
BERMS	Boreal Ecosystem Research and Monitoring Sites
CLASS	Canadian Land Surface Scheme
CLASSIC	Canadian Land Surface Scheme Including Biogeochemical Cycles
COF	Combined Objective Function
FAO	Food and Agriculture Organizations
FC	Field capacity
FroST	Frozen soil temperatures
LAI	Leaf Area Index
LSMs	Land Surface Models
MESH	Modélisation Environnementale communautaire - Surface Hydrology
OA	Old Aspen
OBS	Old Black Spruce
OJP	Old Jack Pine
PET	Potential evapotranspiration
PWP	Permanent wilting point
RMSE	Root mean square error
SABAE	Surface heat and water balances
SHAW	Simultaneous Heat and Water
SpaFHy	Spatial Forest Hydrology

VWC	Volumetric water content
ODE	Ordinary differential equations

LIST OF FIGURES

LIST OF TABLES

1 Introduction

1.1 Background

In semi-arid environments, water loss is dominated by evapotranspiration (ET) (Sun et al., 2010). It is important to quantify ET in semi-arid environments as it affects the ecosystem productivity and energy balance of the region (Lu et al., 2011). Our understanding of ET, particularly in cold regions, is still evolving. (Wang et al., 2017). Since the diversity and number of water-related challenges are large and anticipated to increase in the future, a better understanding of ET can improve water management. Accurately quantifying ET is important for agronomists, soil scientists, and atmospheric scientists.

In higher latitudes and altitudes, winter precipitation is mainly in the form of snow. Thus, water is temporarily stored on the soil surface and is released in spring in the form of meltwater. Part of the precipitation does not reach the soil surface but is caught by vegetation and may be evaporated back to the atmosphere. The remainder will eventually fall to the soil after some delay with the temporary storage. Water infiltrates into the soil to generate subsurface runoff or flows over land as surface runoff into streams. Water evaporates from land. This water vapor rises into the atmosphere and again becomes a source of precipitation. A point scale description of water balance for seasonal frozen soil is displayed in Figure 1.

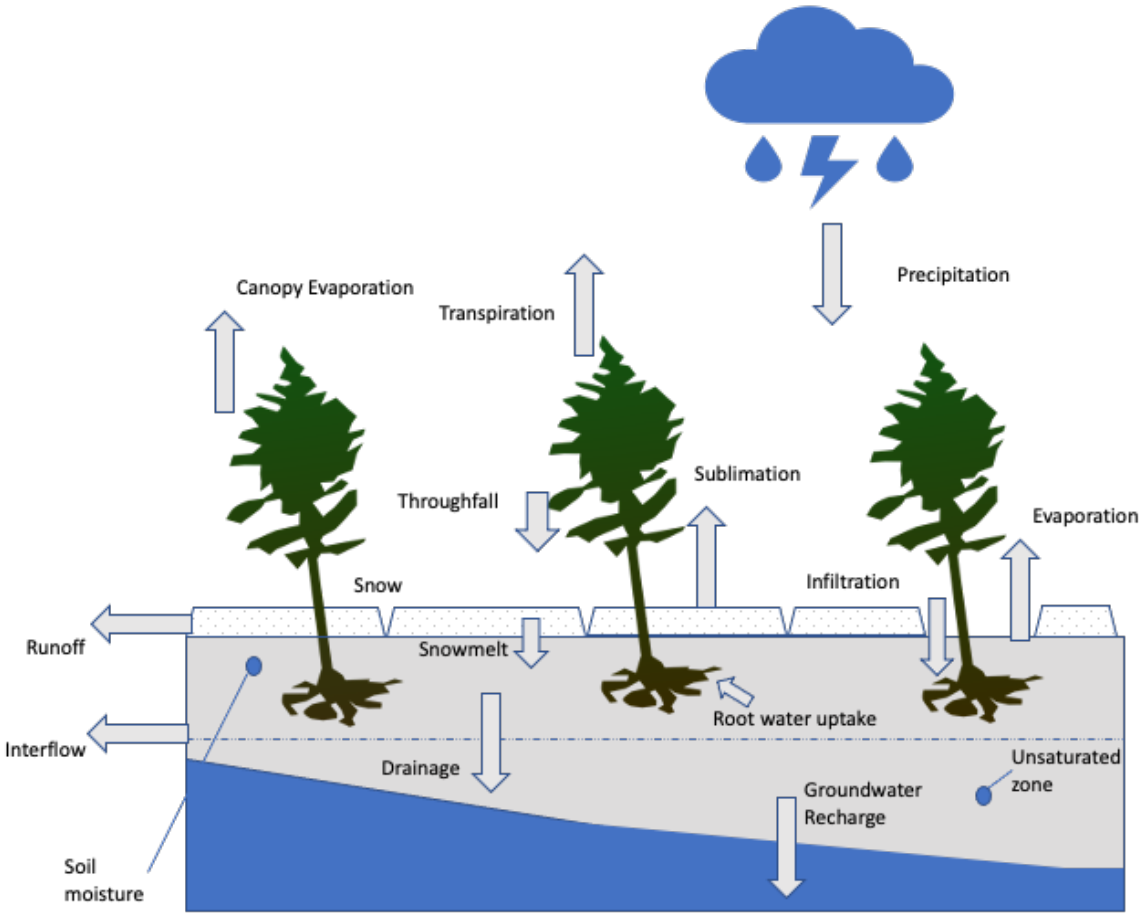

Figure 1: Conceptual model of water balance of a vegetated land surface with fluxes and states

ET is an energy-consuming process. An analytical approach to calculating the rate of evaporation is made through the energy budget. The Law of Conservation of Energy holds that the sinks and sources must be equal in a closed system. Thus, it is possible to deduce ET (known in energy terms as the latent heat flux density) as:

$$\lambda E = K + L - G - H - \frac{dU}{dt} \quad (1)$$

where λE is the latent heat flux density (Wm^{-2}); K is the net shortwave radiation flux density (Wm^{-2}); L is the net longwave flux density (Wm^{-2}); G is the net ground flux density downward (Wm^{-2}); H is the sensible heat flux density (Wm^{-2}); dU is the change in amount of heat stored

in the vegetation and snowpack (Wm^{-2}); and λ is the latent heat of vaporization 2.50 MJkg^{-1} at 0°C.

When there is no water deficit, the rate of ET is mostly controlled by the atmospheric conditions, and ET might be near the maximum energy-limited rate, which is defined as the potential evapotranspiration (PET). However, in the real world, where the water supply is usually limited, the rate of ET is said to be the actual rate of evapotranspiration (AET). The impact of soil moisture on ET is determined by the soil water content and the type of soil (Chaudhury, 1985).

In northern latitudes, hydrological processes are highly dynamic in the spring, during and following the melt period, when most of the runoff and groundwater recharge occurs. Land surface processes are influenced by ice and water, and infiltration in frozen ground is affected by physical and thermal properties of the soil and the rate of snowmelt. During the melt period evapotranspiration (ET) fluxes start to increase in response to higher solar radiation, and photosynthesis resumes in evergreen species. Understanding the impact of frozen soils on hydrological fluxes is important in cold regions, but the effect of frozen soils on plant water uptake is poorly understood. The dynamic interaction between soil water and ET is key to understanding the hydrological balance. In regions with seasonally frozen soils, the soils can remain frozen during snowmelt, and the volumetric water content of (VWC-ice) and liquid (VWC-liquid) of the soils determines the available water for root water uptake. Studies of a sandy upland covered in jack pine in the southern boreal forest have shown that ET is over-estimated in the Canadian Land Surface Scheme (CLASS) at this site. This research extends these previous studies to investigate three sites in the boreal forest in Saskatchewan: Old Jack Pine (OJP), Old Black Spruce (OBS), and Old Aspen (OA).

2 Literature Review

In this research, I seek to improve understanding of infiltration, ET, and runoff during the melt period in boreal forests with seasonally frozen soil. The literature review focuses on identifying current gaps and challenges in quantifying infiltration and ET during the melt period in seasonally frozen soils. The first section describes the governing equations for water movement, the second describes the infiltration process, the third describes the controls on transpiration, and the fourth provides an overview of various Land Surface Models.

2.1 Governing Equations for Water Movement

Soil water storage and flow govern transpiration and control runoff and groundwater recharge. To simulate water transport in soil and understand the flow of soil water in the unsaturated zone, a mathematical model known as Richards' equation is used. Combining Darcy's law and mass conservation equation, Richards (1928, 1931) defined the equation for flow of soil water. Terms can be included in Richards' equation to account for evaporation from bare soil (flux boundary), transpiration from roots (by representing a sink term), infiltration into the soil (a flux boundary condition), and ponding from excess precipitation (a head boundary condition) (Liu et al., 2005).

In a closed volume of soil, conservation of mass holds that the rate of change of saturation (θ) will be equal to the total fluxes (q) going in and out of that volume.

$$\frac{\partial \theta}{\partial t} = -\frac{\partial}{\partial z} q \tag{2}$$

Replacing the q with Darcy's law

$$\frac{\partial \theta}{\partial t} = \frac{\partial}{\partial z}\left[K \frac{\partial h}{\partial z}\right] \tag{3}$$

where K is the hydraulic conductivity, z is the depth below some datum, h is the hydraulic head

The hydraulic head (h) is given by

$$h = \psi - z$$

We get the mixed form of Richards' equation

$$\frac{\partial \theta}{\partial t} = \frac{\partial}{\partial z}\left[K\left(\frac{\partial \psi}{\partial z} - \frac{\partial z}{\partial z}\right)\right] = \frac{\partial}{\partial z}\left[K\left(\frac{\partial \psi}{\partial z} - 1\right)\right] \quad (4)$$

where ψ is the matric potential, t is the time, and z is the depth

Richards' equation can be expressed in three different forms: pressure-head based (ψ-based), water-content (θ-based), and the mixed form (equation 4) (Celia et al.,1990).

pressure-head based

$$C(\psi)\frac{\partial \psi}{\partial t} = \frac{\partial}{\partial z}\left[K(\psi)\left(\frac{\partial \psi}{\partial z} - 1\right)\right] \quad (5)$$

water-content based

$$\frac{\partial \theta}{\partial t} = \frac{\partial}{\partial z}\left[D(\theta).\frac{\partial \theta}{\partial z} - K(\theta)\right] \; ; \; D(\theta) = \frac{K(\theta)}{C(\theta)} \quad (6)$$

where $C(\psi)$ is the gradient of the soil moisture curve

Despite the ease in deriving Richards' equation, it is one of the most challenging equations to accurately and reliably solve in hydrology (Farthing et al., 2017). Solutions to Richards' equation require the relationships of soil parameters such as whether the ψ or the θ-based form are used. Both forms of Richards' equation have advantages and disadvantages to their implementation in a numerical solution. The ψ-based form is more applicable for saturated and layered soil (Huang et al.,1996) but has errors when conserving mass balance. The θ-based form conserves mass balance and enables a faster solution in terms of CPU time, but it does not apply to saturated soils.

2.2 Infiltration

Infiltration plays a key role in partitioning of precipitation at the land surface. By controlling soil water content at the surface (Kim et al., 2017; MacDonald et al., 2017), infiltration affects flooding and stream flow (Garrote and Bras, 1995, Assouline and Ben-Hur, 2006), stored soil water available to vegetation (Verhoef and Egea-Cegarra, 2013), the onset of landslides (Lehmann and Or, 2012), and the exchange of energy and water between atmosphere and soil (Garrote and Bras, 1995). There are no direct measurements of infiltration both empirical and physically based models have been developed to calculate the infiltration rate.

2.2.1 Empirical infiltration models

Empirical models are derived from lab or field observations. These models are mostly simple equations and have a limited physical basis. The parameters are usually obtained by curve-fitting. Many empirical models have been developed to evaluate infiltration and have become popular because of their simplicity and ability to yield reasonable results.

The wide-spread use of Kostiakov models in irrigation is one such example (Ruth et al., 2014). Another empirical infiltration model, FROZEN, was proposed by Zhao and Gray (1999) to estimate snowmelt infiltration from measurable parameters. This algorithm is implemented in the CLASS modelling system as an alternative to the default infiltration algorithm. In this algorithm, a function is derived using the relationship between infiltration, temperature, saturation at the soil surface, total soil saturation and the infiltration opportunity time. The cumulative infiltration is used to estimate the infiltrated water.

$$INF = C\, S_0^{2.92}(1 - S_I)^{1.64}\left(\frac{273.15 - T_I}{273.15}\right)^{-0.45} t_0^{0.44} \quad T_I \leq 273.15 \tag{7}$$

where C is 2.10 for prairie soils and 1.14 for forest soils (Gray et al., 2001), S_0 is the soil surface saturation, S_I is the average soil saturation (ice + water) at the start of the infiltration, T_I is the initial soil temperature at the start of infiltration, INF is the potential infiltration capacity and t_0 infiltration opportunity time

In contrast to these empirical models, with a physically based models, multiple processes, including energy and mass transport can be coupled simultaneously, i.e., energy and mass transport. The most common physically based models are Green-Ampt and Richards' equation.

2.2.2 Physically-based models

Many infiltration equations provide solutions to Richards' equation under ideal conditions e.g., ponded surface, sharp wetting front, and homogenous soil and uniform initial moisture. Eagleson (1970) showed that the Horton Formula can be derived from Richards' equation. Similarly, Philip (1957) converted the Richards' equation into an ordinary differential equation (ODE) and yielded a solution. An exact solution of Richards' equation was also obtained by Green and Ampt (1911) by simplifying the wetting front as a square wave with constant initial moisture content below saturated soil. The Eagleson and Green and Ampt approaches use highly simplified initial and boundary conditions Phillips (1957) also uses these conditions and simplifies the governing equation to remove gravity.

Richards' equation requires initial and boundary conditions to simulate the infiltration (Vereecken et al., 2019). When water starts ponding on the soil surface, infiltration is determined by the hydraulic head at the boundary condition, also known as the Dirichlet boundary condition. When the input water rate goes below the soil infiltration capacity, the Neumann boundary

condition is used in the infiltration, which can be variable or constant. Most Land Surface Models (LSMs) use the Richards' equation to describe the water flow in the soil, but it is primarily used to redistribute water between the soil layers rather than to calculate infiltration rates.

The solution to Richards' equation can require extensive soil property data and fine temporal and spatial discretization, which is computationally expensive. Because certain conditions like soil types and dynamic boundary conditions can present problems of convergence and instability (Gowdish et al., 2009), approximate physically based approaches have been used to model soil water redistribution and infiltration (Haan et al., 1993; Smith et al., 1993; Singh and Woolhiser, 2002). One such approach was made by Green and Ampt (date), who simplified infiltration as a solid wetting front moving downward and considered soil homogenous (see Figure 2). Despite the limitations (assumption of homogenous soil with uniform initial water content and rectangular piston flow) in the Green-Ampt model, their approach is based on fundamental physics and also matches empirical observations. An added advantage of the Green-Ampt's model is that its parameters can be estimated from soil classification (Rawls et al., 1982, 1983).

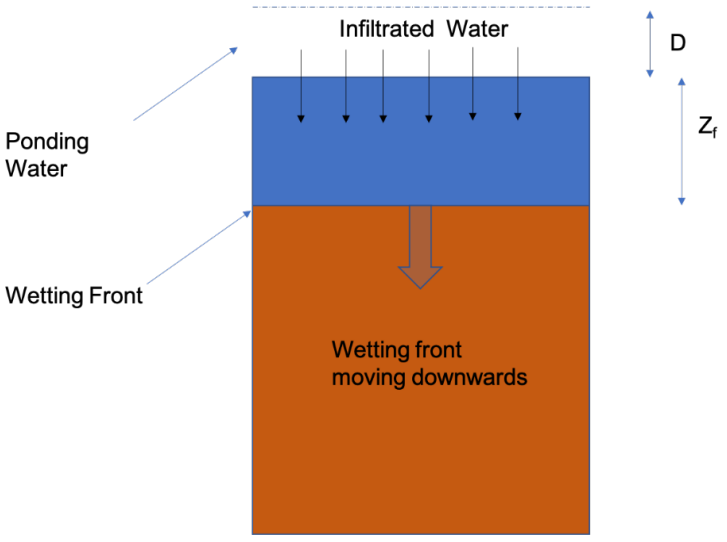

Figure 2: Green and Ampt infiltration as a square wave moving downwards with water ponding at depth D and wetting front at depth Z_f

Although the Green-Ampt model is effective for modelling infiltration into uniform soils, natural phenomena make the model difficult to apply due to the above-mentioned assumptions, including layered soils, surface crusts, and non-uniform initial moisture content, which are regularly encountered in the field. Limitations with the original Green-Ampt model also included difficulties in estimating ponding time and non-steady rainfall. However, modifications to the Green-Ampt model have overcome some of these limitations.

Chu (1978) extended the Green-Ampt model to include non-steady rainfall. For non-homogenous soil, a constant effective hydraulic conductivity was assumed in the extended model (Hachum et al., 1980). Similarly, Beven (1984) represented hydraulic conductivity as a function of depth. The original Green-Ampt model assumed the wetted zone was fully saturated with water (Green and Ampt, 1911). This assumption meant the air was not trapped in the soil and did not affect infiltration. However, trapped air does affect infiltration (Hammecker et al., 2003) and research has been extended to simulate the infiltration into layered soils (Hachum and Alfaro, 1980; Childs and Bybordi, 1969; Selker et al., 1999). Fok (1970) described the infiltration in n soil layers. Flerchinger et al. 1988 further developed the work by forming an explicit equation for infiltration using power series approximation. Chu (1985) extended the Green-Ampt model to three-layered soil, including a tilled layer, a subsoil layer and a crust. Chu (1995) improved the Green-Ampt model parameters for layered soil by including the initial soil water content. Wang (1999) developed a modified Green-Ampt model to describe the infiltration into muddy water for two-layered soil. Chu and Marino (2005) developed a model to simulate infiltration into layered soils for unsteady rainfall and validated with an infiltration experiment for a four-layered field soil profile.

A range of approaches at different levels of complexity exist in infiltration models. Several infiltration approaches address the problems of infiltration capacity, varying soil moisture, spatial

variability, and parametrization of soil properties. Multiple modeling decisions determine how much water is infiltrated into soil (Clark et al., 2008), but the representation varies significantly among different hydrological models.

2.2.3 Infiltration into frozen soil

In cold regions, the melting of snow cover is one of the most important water events of the year. Spring snowmelt partitioning into infiltration and runoff affects solute transport, flooding, and soil moisture for crop production (Appels et al., 2018). The snowmelt rate impacts the infiltration response as it determines the energy and water input in the soil system (Gray et al., 2001). The rate and timing of snowmelt is affected by the energy balance (turbulent flux, radiation flux, ground heat flux, snowpack energy, rain on snow) at the snow surface (Stewart et al., 2009). Snowmelt typically occurs in a diurnal cycle, melting during the day and refreezing at night, a process that influences the infiltration dynamics.

The infiltration of meltwater into frozen soil is a complicated process involving coupled heat and mass flow with phase changes. Therefore, many studies have used numerical models of coupled heat and mass transport to quantify infiltration into frozen soil. 1D numerical models that use coupled mass and heat balance equations (Flerchinger and Saxton, 1989; Zhao and Gray, 1997; Stähli et al., 2001; Hansson et al., 2004) have shown various ways to parametrize the hydraulic properties of frozen soil. One such idea is the use of supercooled soil water by applying the freezing point depression equation. When soil water freezes, the liquid close to soil particles remains in liquid form because of the capillary and adsorptive forces of the soil particles. At subfreezing temperatures, this supercooled soil water is known as the freezing point depression. When ice is

present, the soil water potential is in equilibrium with the vapor pressure. Ignoring the osmotic potential, the matric potential becomes (Fuchs et al., 1978):

$$\psi(T) = \frac{L_f\left(T - T_{frz}\right)}{gT} \tag{8}$$

where L_f is the latent heat of fusion, T and T_{frz} are soil temperature and freezing point, g is the gravitational acceleration.

One possible way to relate soil matric potential to liquid water is

$$\psi(\theta_l) = \psi_{sat}\left(\frac{\theta_l}{\theta_p}\right)^{-b} \tag{9}$$

where θ_p is the porosity of the soil, θ_l is the volumetric liquid water content (Campbell, 1974; Clapp and Hornberger, 1978).

By equating the above two equations, we obtain the $\theta_{liq,max}$, which is the maximum liquid water when the temperature of the soil falls below the freezing point, producing the freezing point depression equation:

$$\theta_{liq,max} = \theta_{sat}\left(\frac{L_f\left(T - T_{frz}\right)}{gT\psi_{sat}}\right)^{-\frac{1}{b}} \tag{10}$$

Frozen soil conditions can reduce the hydraulic conductivity and infiltration rate because the soil pores are blocked with ice (Watanabe et al., 2013). When the soil temperature drops below 0 ^{0}C, some liquid water content is converted to ice within the soil profile. In the soil profile, ice and water coexist because of the freezing point depression (Ireson et al., 2013). At temperatures below the freezing point, matric forces lower the freezing point of water around thinner adsorbed films and small cervices and pores (Spaans et al., 1996). The water in the larger pores freezes at higher temperatures than water in small pores. Since the flow path through the larger pores is severely restricted, tortuosity increases and the infiltration capacity of the soil decreases. Thus, air

enters the larger pores, liquid water the smallest pores, and both liquid water and ice the intermediate pores (Mohammed et al., 2018).

Stähli et al. (1996,1999) quantified the water flow that occurs through air-filled pores during snowmelt infiltration. The study showed that capillary-driven flow was unable to explain this infiltration as the flow was too rapid. Rather, the authors determined that the flow through the larger air-filled pores was more likely to be gravity driven. However, they did not distinguish between macropores and air-filled pores (Stähli et al., 1996; Stähli et al., 1999). Later studies (Bodhinayake et al., 2004) have shown that the macropore network enables a higher infiltration rate. Snowmelt can supply large amounts of water for infiltration, and macropore networks can enable snowmelt to enter deeper soil layers before thawing occurs in the top layer. These macropores help modulate runoff and increase soil moisture storage (Scherler et al., 2010).

When soil freezes, there is a decrease in liquid water content and soil matric potential, leading to a water potential gradient in the soil profile. The water from the deeper, unfrozen soil layers is redistributed to the freezing front. The general tendency is for water to migrate upward toward the downward advancing seasonal frost. As the water from the deeper layer moves upwards, the lower soil temperatures close to the soil surface gradually turn the redistributed liquid water into ice. As a result, hydraulic conductivity of the soil decreases, leading to a further reduction in infiltration.

Several studies (Flerchinger and Saxton 1989; Zhao and Gray 1997; Cherkauer and Lettenmier, 2003) have used this equation to explore water flow in frozen soil. The infiltration capacity is influenced by the ice content and macropores of the soil. However, it can also be affected by the distribution of vegetation, terrain (height and slope), and snow cover (Niu et al., 2006). Several researchers (e.g., Zhao and Gray, 1997; Koren et al., 1999; Stähli et al., 2001; Keith et al., 2003;

Hansson et al., 2004) have used different methods to parameterize the hydraulic properties of frozen soil. Some models (Flerchinger and Saxton, 1989; Hansson et al., 2004) consider the freezing-thawing process to be similar to the drying-wetting process, where the soil matric potential depends on liquid water content. However, Hansson et al., (2004) point out that this method results in a low infiltration rate.

Stähli et al. (2001) proposed that there are two types of flow: high flow through the air-filled pores and low flow through the liquid water close to the soil particles. Cherkauer and Lettenmaier (2003) proposed that the water always finds the path of high infiltration capacity as it travels across a frozen surface. Their macroscale model is split into 10 bins, each with different ice content, which is derived from the spatial distribution of soil temperature. This model increased the infiltration rate and performed well in large-scale processes.

The thermal and hydrologic properties of soil change in the presence of ice. LSMs that can explicitly represent the frozen soil can improve simulation of soil water storage and runoff. To improve the simulation of infiltration in the models, several key issues need to be addressed: the rate of infiltration into frozen soils; the timing of infiltration into frozen soils from snowmelt; the conditions that allow the water to infiltrate into deeper layers bypassing the frost zone; and the refreezing of the infiltrated water. A better understanding of these issues can improve the infiltration model, but it is also important to improve our knowledge of plants' ability to access soil water from frozen soils. Plants respond to both the magnitude and timing of soil moisture and temperature (Bonan and Shugart, 1989). The thawing of frozen soil occurs in conjunction with changes in soil temperature and soil water content, both of which play an important role in boreal plant transpiration.

2.3 Controls on transpiration

Plants absorb water and nutrients from their roots. Used for physiologic and metabolic function, water is released as a vapour via the stomata on the leaves. This transport of water from roots to leaves through plant tissues is called transpiration. Vegetation has a strong influence on ET.

Vegetation type can alter the whole hydrological cycle (Ireson et al., 2015). Leaf Area Index (LAI), canopy structure, root length has a direct impact on transpiration, and it greatly differs with vegetation type. Needle-leaf trees (i.e., OBS, OJP), or conifers, have leaves in the form of needles year-round (Peters et al.,2010). On the other hand, during fall, broadleaf trees (i.e., OA) lose their leaves necessary to capture sunlight and enter winter dormancy. Coniferous forests intercept 60% of snowfall and 25–45% of the snow can be lost because of sublimation from the canopy (Pomeroy et al.,1998). For example, snow cover is less in coniferous forests than in deciduous forests and open areas. Additionally, the forest canopies lower the intensity of shortwave radiation. As a result, the melt of ground snowpack is slower in coniferous forest. Evergreen needle-leaf trees tend to have lower leaf transpiration rates, a longer leaf lifespan, a higher leaf area index, and longer active growing seasons than do deciduous broadleaf trees.

The hydrological process is intimately linked to the forest canopy as it influences energy exchange with the atmosphere and the land surface (Varhola et al., 2010). Forested areas accumulate less snow than open areas; however, compaction occurs when snow drops from the canopy, leading to an increase in the density of the snow compared to the open areas. Additionally, since snow is protected from turbulence and snow radiance, it remains on the ground until the spring.

Although models of vegetation play a significant role in advancing the understanding of ET processes, hydrological models often ignore the vegetation characteristics in the parameters related to ET. The different types of land cover in the Boreal Plain ecozone (BPE) results in varying

ET rates. Diverse vegetation and soil water capacity impacts the evaporation rate in this region. Needleleaf transpires 2–3 mm d^{-1} and deciduous transpire 5 mm d^{-1} because the evergreen has a lower leaf area index (LAI) (Zha et al., 2010).

2.3.1 Stomatal and Canopy Conductance

Stomatal conductance controls the rate of water vapor exiting or CO_2 entering a plant through stomata (Zhu et al., 2018). Stomatal conductance can be used as an indicator of plant water status. Stomata also regulate transpiration-driven water flow (Damour et al., 2010). The ease with which water flows through the plant can be expressed quantitively by the following equation.

$$F = C\Delta P \tag{11}$$

where F is the flow of water through the plant, ΔP is the water potential gradient between the soil and plant shoot, and C is hydraulic conductance in the liquid phase only, so pertains to the soil-plant continuum.

The availability of instruments like gas exchange analyzers and diffusion porometers has enabled the measurement of leaf stomatal conductance (g_s) in field conditions and investigation of the variables that affect this parameter (Gerosa et al., 2012). However, such measurements of are only possible when foliage is dry. Additionally, remaining a long time in the measurement chamber may affect the physiological state of leaves. Alternatively, a mathematical model that connects stomatal function to plant attributes and environmental variables would be helpful in predicting stomatal behaviour. Historically, stomatal conductance has been quantified using empirical models (Jarvis, 1976). The empirical mechanism includes two variables: turgor pressure or guard cell and osmotic pressure or osmotic content. In this approach, the rationale is that the aperture in stomata increases when the volume of guard cells increases (Buckley et al., 2017), which

occurs because of osmotic water movements. Turgor or guard cells are predicted with the help of the mass balance, based on the assumption that a steady-state balance guides the water potential between evaporative water loss and the water supply in plants or leaves (Chabrand et al., 2017).

Canopy conductance (r_c) is calculated by scaling leaf stomatal conductance while treating the canopy as one big leaf (Dingman et al., 2014). Half of the total green leaf area per unit of ground surface area (Chen et al., 1992), LAI is a dimensionless quantity that is used to characterize plant canopies. A maximum unstressed canopy conductance $r_{c,max}$ is scaled by the ratio of the actual leaf area index (LAI) to the maximum (LAI_{max}) for that canopy type:

$$r_c(LAI) = r_{c,max} \frac{LAI}{LAI_{max}} \tag{12}$$

where LAI is defined as one half the total green leaf area per unit ground surface area and $r_c(LAI)$ is the unstressed composite canopy conductance.

The stomatal conductance model developed by Jarvis (1988) is an empirical model based on the response of canopy conductance to environmental factors. The model incorporates the response of (g_s) to leaf temperature, light intensity, vapour pressure deficit, CO_2 concentration, and leaf water potential (Gerosa et al., 2012). Verseghy et al. (1993) use a similar experimental relationship in CLASS, where the factors represent the environmental stress effects of stomatal control (see Figure 3):

$$r_c = r_c(LAI)\, f_1\, f_2\, f_3\, f_4 \tag{13}$$

where $r_c(LAI)$ is the unstressed composite canopy conductance

f_1 is a function of solar radiation, K (Wm^{-2}),

$$f_1(K) = \max\left(1.0, \left(\frac{500}{K} - 1.5\right)\right) \tag{14}$$

f_2 is a function of vapor pressure deficit Δe (mb)

$$f_2(\Delta e) = \max\left(1.0, \left(\frac{\Delta e}{5}\right)\right) \tag{15}$$

f_3 is a function of soil moisture potential, ψ (m) (Campbell,1974).

$$f_3(\psi) = \max\left(1.0, \left(\frac{\psi}{40}\right)\right) \tag{16}$$

f_4 is a function of temperature, T (°C) that ranges from 0 to 40°C:

$$f_4(\mathrm{T}) = 1.0 \; if \; T < 40 \; and > 0 \; ℃$$

$$if \; T > 40℃ \; or < 0 \; ℃ \; then \; f_4(\mathrm{T}) = \frac{5000}{r_c(LAI)} \tag{17}$$

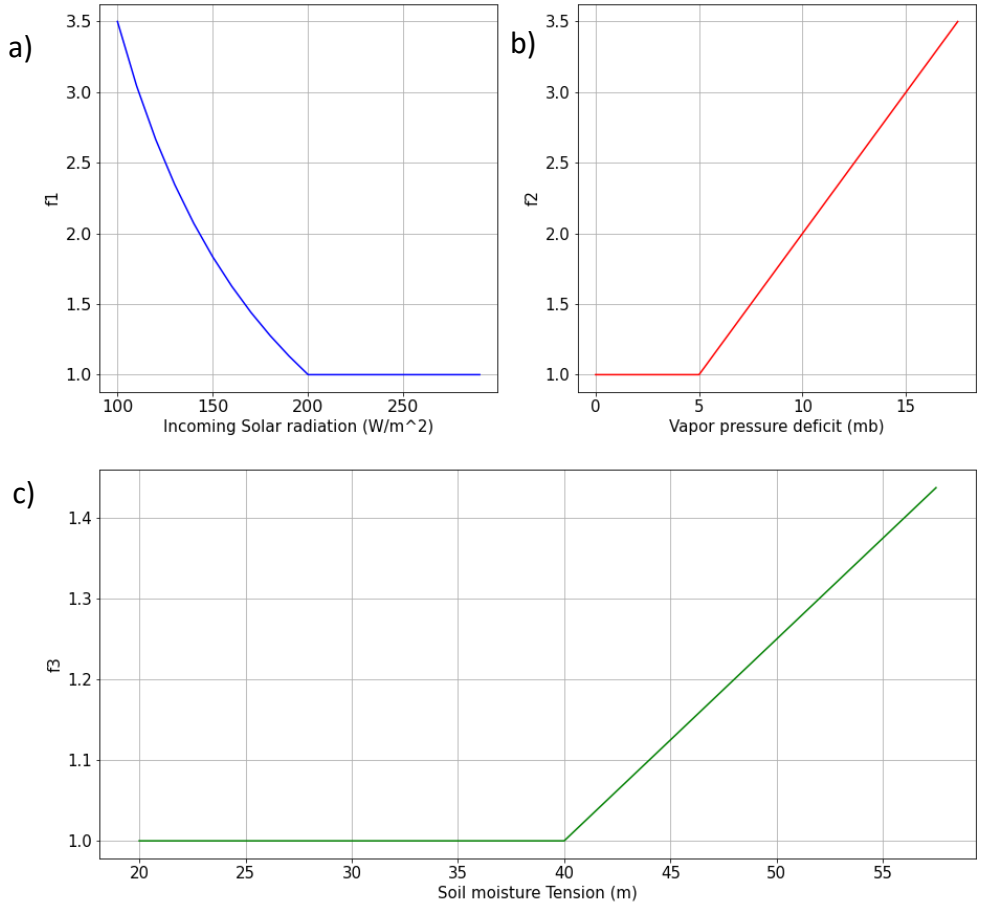

Figure 3: Effect of environmental stress a) solar radiation (top left), b) vapor pressure deficit (top right), c) soil moisture tension (bottom) on stomatal resistance.

One criticism of this model approach is that the synergistic interactions between the environmental factors are not considered (i.e., the model supposes that the response of each factor is independent). However, interactions between factors are reported, for example, the relationship between vapor pressure and soil moisture (Tardieu et al.,1996).

Samuli et al. (2019) proposed vegetation variability in a model to understand the strong influence of vegetation on ET by coupling canopy radiation transfer to leaf-scale stomatal conductance. The research uses a Spatial Forest Hydrology (SpaFHy) framework, and the model output (specific discharge and ET) is well predicted. SpaFHy was able to reproduce ET, measured by the eddy covariance method in Finland and Sweden, reasonably well at stand scale. The sensitivity analysis in the research showed that the LAI is the main parameter affecting ET. For this reason, it is important that the LAI is accurate to obtain an accurate estimation of ET.

2.3.2 Root uptake models

In a simple lumped soil profile uptake model, the amount of water available for plant uptake is dependent on the soil volumetric water contents at the permanent wilting point (PWP) and field capacity (FC). The PWP and FC are in turn related to soil water potential (O'Geen, 2013). As water content decreases in a soil profile, the matric potential also decreases, and, as a result, the remaining water is held more strongly. Soil moisture content between saturation and field capacity is transitory. This water is subject to free drainage and thus unavailable for plants. The soil moisture that is held between FC and PWP is available for plants for transpiration. Although water held between these two points is retained against gravity, it but can still be extracted by plants. At the PWP, the matric forces hold water too tightly to be available for plants.

Physically based root water uptake models are generally classified into two approaches: microscopic and macroscopic, based on how the uptake term is handled. Microscopic models of water flow describe water flow from the soil to and through the plant roots. The microscopic approach generally involves descriptions of radial flow to, and uptake by, individual roots (Hillel et al., 1975). The appropriate form of a flow equation for a microscopic approach can be represented in cylindrical coordinates (Kumar et al. ,2014).

$$\frac{\partial \theta}{\partial t} = \frac{1}{r}\frac{\partial}{\partial r}\left(D\frac{\partial \theta}{\partial r}\right) \tag{18}$$

where D is the soil moisture diffusivity, and r is the radial distance from the axis of the root.

In contrast, the macroscopic approach consists of a root system with an uptake term that sums up the effects of all individual roots. In the macroscopic approach, the extraction of water from the soil layers by ET can be numerically modelled by adding a "sink" term, S, to Richards' equation to represent uptake of water.

$$\frac{\partial}{\partial z}\left[K(\psi)\left(\frac{\partial \psi}{\partial z} - 1\right)\right] - S = C(\psi)\frac{\partial \psi}{\partial t} \tag{19}$$

Feddes et al. (1976) described a water uptake model that describes transpiration that depends on soil moisture conditions of the soil profile. The sink term (S) is related to potential transpiration (T_p).

$$S(\psi, z) = r_s(\psi) r_d(z) T_p(t) \tag{20}$$

where $r_d(z)$ is the root density distribution function and, $r_s(\psi)$ is the water stress function

The root density distribution is calculated using the following equation.

$$\int_0^{L_r} r_d(z)dz = 1 \tag{21}$$

where L_r is the root length

The water stress function is calculated by the relationship

$$r_s(\psi) = 0 \qquad \psi > \psi_{an} \tag{22}$$

$$r_s(\psi) = 1 \quad \psi_{an} \geq \psi > \psi_d$$

$$r_s(\psi) = 1 - \frac{\psi - \psi_d}{\psi_w - \psi_d} \quad \psi_d \geq \psi > \psi_w$$

$$r_s(\psi) = 0 \quad \psi_w \geq \psi$$

where ψ_w is the matric potential threshold for PWP, ψ_d is the matric potential threshold below which water stress starts to occur, and ψ_{an} is the matric potential threshold above which the soil is too wet to extract water. The details of different root water uptake models are illustrated in Table 1.

Table 1: Brief overview of sink term (S) used in the root water uptake models

Name of Model	Equation used	Parameter used
Molz and Remson	$S = \frac{TL(z)D_s(\theta)}{\int_0^v L(z)D(\theta)dz}$	Soil water diffusivity (Molz et al., 1970)
Perrochet	$S(\psi, z) = \alpha(\psi)g(z)T_p$	Root distribution function (Perrochet, 1987)
Jervis	$S_i = \frac{E_g}{\Delta Z_i}\left\{\frac{R_i\alpha_i}{\alpha}\right\}$	Actual transpiration rate, soil layer (Jervis, 1989)
Kang	$S(z,t) = f(\theta)T_p(t)\frac{1.80e^{-\frac{-1.8z}{z_r}}}{(1-e^{-1.80})\,z_r}$	Potential transpiration and effective root zone depth (Kang et al., 2001)

The macroscopic approach has significant advantages over the microscopic approach (Kumar et al., 2013). First, it does not require complete knowledge of the physical processes of root water uptake, so the need for complex parameters such as root permeability, root length density

and root water potential that are difficult to estimate are eliminated. Microscopic models are preferred when physiology is the focus of the research. In the microscopic approach, the model can include the interactions between the plant and its environment. However, microscopic models, such as the root architectural model, are challenging to parametrize. Microscopic models use cylindrical coordinates to solve the boundary conditions at the root surface (Li et al., 2001). The geometry of a growing root is expensive to measure, and the water permeability also varies along the position of root, so this model is not the most practical for all uses. Consequently, macroscopic approaches are generally favored in soil water simulation models.

2.4 Overview of Land Surface Models

Land Surface Models have evolved substantially over the past few decades, with finer spatial resolution and higher computing capabilities. Many studies have applied LSMs to simulate water fluxes and the surface energy balance. Advances in the fields of meteorology, hydrology, and soil physics are making LSMs more physically based. Recent studies have shown that to estimate ET, LSMs must accurately simulate soil and snow processes (Ukkola et al., 2016).

Accurate simulations of soil temperature and moisture profiles are crucial for modelling processes like ET, root growth, and root water uptake. In the boreal forest, cold soil temperatures contribute to ice formation within the soil, and snowmelt contributes to the springtime runoff and streamflow. Soil profiles also vary greatly with depth and terrain. Thus, it is crucial that the models applied to the seasonally frozen soils be comprehensive. Levine et al. (1997) developed a soil model FroST (frozen soil temperatures) to predict soil moisture and temperature at various depths, which was tested at the Boreal Ecosystem Research and Monitoring Sites (BERMs) sites. FroST underestimated the soil temperature for each depth, and the difference was greatest when snow

was present. The study reported that the parameterization of canopy characteristics in the FroST setup does not correctly estimate the thermal properties of the canopy.

Local changes in hydrothermal properties below and above ground can change the extent of heat retention and water and frost penetration. Various processes like ET, root growth, and root water uptake are all impacted by local changes in soil moisture and temperature conditions. The changes in soil temperature and moisture impact forest productivity by limiting water, energy, and nutrients. Balland et al. (2006) applied the ForHym model to three study sites: Old Jack Pine (OJP), Old Black Spruce (OBS), and Old Aspen site (OA) to calculate snowpack depth and density, canopy interception, frost depth soil moisture, and temperature at any depth. The model simulation of unfrozen soil moisture content did not agree with the field data, and soil moisture was overestimated in summer and underestimated in winter (Bhatti et al., 2006).

Previous studies have defined potential evaporation as the ET for well-watered short grass or evaporation from a free water surface (Milly et al., 2016; McMahon et al., 2013). However, in the presence of snowpack, these past methods overestimate potential ET. Neto et al. (2020) presented a new definition of potential evaporation that accounts for the presence of snow in the land surface. In their study, PET in a landscape that has partial snow coverage is defined as the "maximum water evaporation from an unstressed water surface covered by unstressed snow surface," and the snow coverage changes seasonally (Neto et al., 2020, p2).

Hejazi et al. (2011) performed a model evaluation using surface heat and water balances (SABAE) by comparing temperature and soil moisture from the BERMS field sites. SABAE simulated soil temperature and snow depth well, but the simulated soil temperature in winter showed some discrepancies. Additionally, there was no general agreement about liquid soil moisture, particularly at lower depths. Chen et al. (2016) incorporated an organic soil layer in the LSM (Noah-

MP) to understand its impact on the water cycle and surface energy components of OA. The inclusion of organic soil layers in improved the simulated latent and sensible heat fluxes during the spring soil thaw.

A study was conducted to evaluated eight LSMs across six towers to understand ET during droughts (Ukkola et al., 2016). The results showed that the LSMs overestimate the magnitude, intensity, and duration of actual ET when compared against the flux tower measurements. There were clear deficiencies in simulating ET at most sites, with the best performing models overestimating by 12-14%. There is a need to re-examine existing components of LSMs to improve the simulation of heat and water fluxes. Representation of plant water stress and soil hydraulic properties were considered important in determining ET in this study.

Sun and Verseghy (2019) found that CLASS overestimated ET for mid-latitude shrublands due to overestimation of soil evaporation during the wet periods in spring. This depletion of soil water in spring resulted in underestimation of ET in the summer. To improve the representation of surface-atmospheric atmosphere interaction in Canadian Land Surface Scheme Including Biogeochemical Cycles (CLASSIC), Meyer et al. (2021) added a modification that dictates the efficiency of water evaporating from the soil surface. This improved the high bias from ground evaporation in the model. Nazarbakhsh et al. (2020) hypothesized that excessive infiltration into frozen soil in CLASS might have led to an overestimation of ET during the melt period in the OJP site. A constant theme across models and sites is the overestimation of simulated ET, particularly during the spring period.

A good performance with respect to the calibration variable but a reduced performance in the other variables is not ideal in LSMs. This study aims to improve the performance of the ET fluxes, in conjunction with that of other hydrological fluxes. During the last few decades,

developments in approaches used in model calibration have improved land surface model predictions. Physically based land surface models require numerous soil and vegetation parameters to balance the water and energy processes (Crow et al., 2003). Parameter selection complexities are often compounded by the land surface heterogeneities. Many parameters like stomatal resistance, surface roughness length, and vegetation root depth are difficult to estimate at both small and large spatial scales. Thus, physically based models require calibration to improve representation of land surface fluxes and state variables. Ireson et al. (2021) showed that a single objective calibration using soil moisture alone cannot guarantee adequate calibration and the fluxes are subject to high uncertainties.

2.5 Summary

In regions with seasonally frozen soils, the soils remain frozen during snowmelt, and the ice and liquid water content of the soils determines the soil hydraulic properties and partitioning of snow-melt between infiltration and runoff. The hydrological fluxes are highly dynamic during the melt period, when ET also increases. The impact of frozen soils on plant water uptake is still poorly understood. This literature review has presented an overview of hydrological processes in forests with seasonally frozen soils and identified the challenges involved with improving the predictions of ET and infiltration. As shown in the literature review, LSMs have failed to simulate ET and infiltration accurately. Nazarbakhsh et al. (2020) hypothesized that infiltration is overestimated in frozen soil results leads to the ET model bias in spring. The current study first conducts numerical experiments to improve understanding of water uptake in CLASS. Second, the study performs a calibration study at the three boreal sites and evaluates the performance in replicating the observed fluxes and states. The research study intends is to produce estimates of the hydrological fluxes with high confidence. Thus, a multi-objective calibration is performed to better constrain the fluxes and states in the model.

3 Statement of Research Purpose and Objectives

The purpose of the research is to improve understanding of infiltration, ET, and runoff processes in forests with seasonally frozen soil. The specific objectives of the research are as follows:

Objective 1: Undertake baseline model runs using CLASS for three seasonally frozen sites: OJP, OBS, and OA, and document the ability of the model to simulate ET by comparing these simulations with field observed data at each site.

Objective 2: Use numerical experiments with CLASS to learn in detail how the simulated hydrologic fluxes respond during and after spring thaw under different parameter sets and critique the model performance based on the current physical understanding.

Objective 3: Compare model performances and evaluate uncertainty under single and multi-objective calibration.

4 Method

4.1 Study Sites

The field sites Old Black Spruce (OBS), Old Jack Pine (OJP) and Old Aspen (OA) are located in the southern boreal forest in central Saskatchewan. These are Boreal Ecosystem Research and Monitoring sites (BERMs), which have been extensively and continuously monitored since the mid 1990s. The three BERMS sites cover three different types of vegetation. The dominant species at OJP is Jack Pine, OA is Trembling Aspen and OBS is Black Spruce. OBS and OJP are conifers and OA is broadleaf. The terrain of this area has a mean elevation of 520 m and is generally flat (Bhatti et al., 2006; Bartlett et al., 2003; Barr et al., 2012). OBS (54.0 N, 105.10 W) is located near White Swan Lake, and the dominant forest vegetation is black spruce. The soil is covered with a 20 to 30 cm peat. The peat layer forms the understory, and this site has poorly drained soil. OJP (53.60 N, 104.70 W) is located near Narrow Hills Provincial Park. The sandy soil is well drained, and the dominant forest vegetation is jack pine. OA (53.60 N, 106.20 W) is located near the south end of Prince Albert National Park in Saskatchewan on loamy soil. The dominant forest vegetation is trembling aspen. Ground level vegetation consists of beaked hazelnut and alder, and the soil is moderately well drained. The sites have flux measurements (water, energy, and carbon fluxes) and meteorological measurements.

In the three boreal forest study sites, the soil freeze-thaw process significantly influences the hydrological cycle and forest ecosystem, as it does in the entire region. The seasonally frozen soil in these sites provides an ideal opportunity to understand ET, infiltration, and runoff processes during the melt period. The site selection was based on the availability of long data sets (1997–2015) and the uniform land cover. The site also provided an opportunity to analyze the various fluxes across contrasting species at different sites that have a similar climate. These sites started

as the Boreal Ecosystem-Atmosphere Study (BOREAS) in 1994, and since 1997, they have continued as part of Boreal Ecosystem Research and Monitoring Sites (BERMS). The site descriptions are provided in Table 2 (Wu et al., 2013).

Table 2: Study site description (Barr et al., 2012; Pan et al., 2017)

Characteristics	Old Aspen	Old Black Spruce	Old Jack Pine
Location	53.269 °N, 106.200°W	53.987°N, 105.117°W	53.916°N, 104.690°W
Elevation(m ASL)	600.6	628.9	579.3
Ground cover	dense hazel	exposed soil moss, herbs	lichen, exposed soil
Dominant tree species	Trembling Aspen	Black Spruce	Jack Pine
Vegetation Type	Deciduous Broad-leaf	Evergreen Needle-leaf	Evergreen Needle-leaf
Stand density (trees ha^{-1})	980	4330	1320
Canopy height	21m	11m	14m
Soil Layer	Mineral Soil: Loam to clay Organic soil: Litter, fibric and humic	Mineral Soil: Sandy clay Organic soil: Peat, mosses and lichens	Mineral Soil: Fine sand
Drainage	Good to moderately good	Imperfect to poor	Very good

4.2 Instrumentation and Data

The measurement height/depth and instrument used for half hourly forcing data to run the model are summarized in Table 3. Accumulating gauge was used to measure the precipitation at OA, OBS and OJP and is located in the centre of small forest clearings. Eddy-covariance measurements of half hourly ET (Barr et al., 2006, 2012) were made from scaffold towers and were used to test the performance of the model. The half hourly VWC-liquid data is available at various depth at the three sites as listed in Table 3 is also used to assess the model performance. We used these data

to estimate the VWC-liquid data at model depths for calibration and validation. The forcing and the validation data from 1999 to 2015 were used in this study for analysis and modelling purposes. Data from the flux towers were pre-processed, WISKI database handled real time collection and processing of the data. The forcing data and observed data used for this research were already post-processed and downloaded from the "summary" timeseries in the WIKSI database. The driving data showed diurnal, seasonal, and interannual variation in the dataset.

Table 3:Instrumentation at field sites (Pan et al., 2017; Barr et al., 2012)

Variable	OJP	OBS	OA
Air temperature (°C) and Relative humidity (%)	Vaisala HMP45C 14 m above canopy	Vaisala HMP45C 14 m above canopy	Vaisala HMP45C 16 m above canopy
Wind speed (m/s)	CS CSAT3 tri-axial sonic anemometer above canopy	Gill R3 or R3-50 tri-axial sonic anemometer above canopy	Gill R3 or R3-50 tri-axial sonic anemometer above canopy
Solar radiation (W/m^2)	Kipp and Zonen CM11 paired pyranometer 9-14 m above canopy	Kipp and Zonen CM11 Paired pyranometer 9-14 m above canopy	Kipp and Zonen CM11 paired pyranometer 10-16 m above canopy
Longwave radiation (W/m^2)	PIR paired pyrgeometer 9 -14 m above canopy	PIR paired pyrgeometer 9 -14 m above canopy	PIR paired pyrgeometer 10 -16 m above canopy
Precipitation (mm)	Belfort 3000 accumulating gauge	Belfort 3000 accumulating gauge	Belfort 3000 accumulating gauge
Volumetric water content (m^3/m^3) Depths (cm bgl)	CS615 water content reflectometers 0–15, 15–30, 30–60, 60–90, 90–120, and 120-150 cm	CS615 water content reflectometers 2.5, 7.5, 22.5, 45 and 60-90 cm	Time domain reflectometers 0–15, 15–30, 30–60, 60–90, and 90–120 cm
Soil Temperature (°C)	Cu-Co Thermocouple sensors 2, 5, 10, 20, 50 and 100 cm	Cu-Co Thermocouple sensors 2, 5, 10, 20, 50 and 100 cm	Cu-Co Thermocouple sensors 2, 5, 10, 20, 50 and 100 cm

4.3 Model Description

The study applied offline CLASS in a point mode. CLASS is a land surface parameterization scheme for large scale climate models that use physically based equations to calculate the water and energy balance of the land surface (Bartlett et al., 2003). It is specifically designed to simulate the effects of soil, vegetation, and snowpack on the physical exchanges between the land and atmosphere. It uses atmospheric data to drive the calculation.

A grid cell in CLASS can include four sub areas: bare soil, snow-covered soil, vegetation, and snow on vegetation patches. Seven meteorological forcing variables: precipitation, air temperature, incoming shortwave radiation, incoming longwave radiation, wind speed, specific humidity, and pressure are used to drive the moisture and energy balances of each sub area. The initial version of CLASS divided the soil into three-layer depths: 0.1, 0.25, and 3.75 m thickness, but the latest version has a flexible soil layering scheme.

The vegetation types in the model are divided into four main groups: deciduous trees, coniferous trees, crops, and grass. The canopy interception capacity is a function of the LAI. Transpiration is dependent on canopy stomatal resistance, which is a function of soil moisture tension, temperature, atmospheric vapour pressure deficit, incoming solar radiation, and the LAI.

4.4 Baseline model configurations

Baseline runs provide an opportunity to explore whether CLASS with a priori parameter values can replicate observed ET or if parameter calibration is needed. Three main types of data required to run the model were considered: time-series atmospheric forcing data, parameter values describing the vegetation, parameter values describing the soil properties. The baseline models were run on a half hourly time-step from August 1, 1997 to September 30, 2010 with observed meteorological forcing data at the three sites. The instruments and measurements for the forcing data are

explained in Section 4.3. Parameters that described the vegetation and soil at each site (e.g., leaf area index, canopy mass, and rooting depth) were taken from previous research at the sites (Chen et al., 2006; McCaughey et al., 2006; Isabelle et al., 2018; Ireson et al., 2021; Table 4). CLASS documentation was used for the parameters that were not described in the literature. The parameters used for the baseline run are displayed in Table 4. Canopy height was based on the height of the flux towers. The soil column was divided into three soil layer depths with thicknesses of 0.1, 0.25, and 4.1 m (Bartlett et al., 2006).

Table 4: Baseline CLASS parameters (FP – fibric peat organic soil layer)

Parameter	OJP	OBS	OAS
Needle leaf fraction of grid-cell	1.0	1.0	0.0
Broadleaf fraction of grid-cell	0.0	0.0	1.0
Canopy height (m)	28	28	28
Leaf Area Index minimum	2.7	2.56	4
Leaf Area Index maximum	2.7	2.56	1
Sand percent in layer 1, 2, 3	93,93,93	FP,93,93	FP,93,93
Clay percent in layer 1, 2, 3	3,3,0	0,3,3	0,3,1
Organic percent in layer 1, 2, 3	2,2,2	0,2,2	0,2,2
Rooting Depth (m)	1	1	1

Soil hydraulic properties in CLASS are based on pedotransfer functions by Cosby et al (1984). The hydraulic properties were calculated from soil texture (sand and clay percentages).

$$\theta_p = \frac{-0.126X_{Sand} + 48.9}{100.0} \quad (23)$$

$$b = 0.159\, X_{Clay} + 2.91 \quad (24)$$

$$\psi_s = 0.01\, e^{(-0.0302 X_{Sand} + 4.33)} \quad (25)$$

$$K_s = 0.60960384 e^{(0.0352 X_{Sand} - 2.035)} \quad (26)$$

where X_{Sand} (%) is sand percentage, X_{Clay} (%) is the clay percentage of the soil layer, K_s (m/s) is the saturated hydraulic conductivity, θ_p is the porosity, and b (-) is a shape parameter.

Previous CLASS simulation at OBS and OA showed that the top 10-cm layer contains an organic soil layer (Bartlett et al., 2006). The use of a fibric peat organic layer in CLASS modifies the hydraulic properties of that soil layer and is summarized in Table 5.

Table 5: Hydraulic properties of fibric peat soil layer (Letts et al., 2000)

Hydraulic Properties	Fibric peat
θ_p	0.93
b	2.7
ψ_s	0.0103
K_s	2.8×10^{-4}

Three years of data, starting on August 1, 2006 (under snow-free conditions) were given as spin up for initializing CLASS simulation, thus allowing the model to eliminate the effect of the initial conditions of soil moisture and soil temperature. The model initial VWC-liquid and soil temperature was based on observed estimates. For the baseline configuration, the daily simulated ET outputs were compared from October 1, 2009 to September 30, 2010 to daily observed ET data from flux towers.

4.5 Numerical Experiments

In this section, we present a series of numerical experiments to gain insight into the simulated infiltration and ET fluxes in CLASS. In each case, controlled initial and boundary conditions are used to isolate specific processes, and a hypothesis is provided for each numerical experiment, which reflects the understanding of how the real-world system works. By comparing the actual outcome with the hypothesis, we may be able to learn something about how the model works and may also raise questions about how the real-world system works.

4.5.1 Infiltration into unfrozen and frozen soil

Hypothesis: Infiltration does not occur if the first soil layer is frozen and saturated.

In this experiment, we were interested in how potential infiltration (PI) is partitioned between infiltration and runoff. Since PI is snowmelt + rain on the ground, the easiest way to simulate this was by an artificial rainfall pulse that is applied to the model with no snow on the ground. We considered different soils, different precipitation intensities, and different degrees of ice/liquid water content. Sixty-four combinations were studied, which included two different types of soil (sandy and clayey); half hourly eight different PI intensities (m) (0.0001, 0.0003, 0.0005, 0.001, 0.003, 0.005, 0.007 and 0.01), all with a one-day duration; and four different initial VWC-liquid and VWC-ice combinations, as presented in Table 6. The premise for selecting the VWC-liquid and VWC-ice (Table 6) combinations was to test infiltration into i) a frozen and saturated top soil layer, ii) a frozen and saturated first and second soil layer, iii) a frozen and saturated first, second, and third soil layer; and iv) unfrozen soil. The porosity of the sandy and clayey soil, described in this experiment, is 0.37 and 0.43 respectively and is calculated using the pedotransfer function described in section 4.4. Since the residual soil liquid water content for mineral soil after freezing

or evaporation is 0.04, the saturated VWC-ice for a sandy and clayey soil is 0.33 and 0.39 respectively (Verseghy, 2012).

The drainage parameter was set to zero, so there was no drainage. The LAI min and LAI max were both set to 0.1, so there were no negligible ET losses. Neglecting the effect of drainage and ET helps to simplify the soil water balance (i.e., change in storage will be approximately equal to infiltration) and to understand where the water enters after infiltration occurs in the soil without losses from drainage and ET. Change in liquid water storage (ΔS_j) was calculated in units of depth of liquid water equivalent, by depth integrating the VWC-liquid (θ_L) in equation 27 (Nazarbaskh et al., 2020).

$$\Delta S_j = \sum_{i=1}^{3} \left(\theta_{Li,j} - \theta_{Li,j-n}\right) \Delta z_i \tag{27}$$

where i and j are indices in depth and time, respectively, Δz_i (L) is the layer thickness, and n is the index to calculate the storage at various time steps. The time-integrated infiltration flux is given by

$$I = \sum_{i=1}^{nt} (R_i - RO_i) \Delta t \tag{28}$$

R_i is the model output rainfall (throughfall), RO_i is the model output runoff, and Δt is the model time step (30 minutes)

Table 6: Model setup to understand infiltration in CLASS by changing initial VWC -liquid and VWC-ice, and applying an artificial rainfall pulse

Porosity (1st, 2nd, 3rd layer): 0.37/0.37/0.37 (sandy soil at OJP)			
Scenarios	Time Period Considered	Ice Content (1st, 2nd, 3rd layer)	Liquid Water Content (1st, 2nd, 3rd layer)
1	2011-05-16 - 2011-05-17	0.33/0.23/0.006	0.04/0.04/0.12
2	2011-05-16 - 2011-05-17	0.33/0.33/0.006	0.04/0.04/0.12
3	2011-05-16 - 2011-05-17	0.33/0.33/0.33	0.04/0.04/0.04
4	2011-06-17 - 2011-06-18	0.0/0.0/0.0	0.2/0.2/0.2
Porosity (1st, 2nd, 3rd layer): 0.43/0.43/0.43 (clayey soil at OBS)			
Scenarios	Time Period Considered	Ice Content (1st, 2nd, 3rd layer)	Liquid Water Content (1st, 2nd, 3rd layer)
5	2011-05-16 - 2011-05-17	0.39/0.23/0.006	0.04/0.04/0.12
6	2011-05-16 - 2011-05-17	0.39/0.39/0.006	0.04/0.04/0.12
7	2011-05-16 - 2011-05-17	0.39/0.39/0.39	0.04/0.04/0.04
8	2011-06-17 - 2011-06-18	0.0/0.0/0.0	0.2/0.2/0.2

4.5.2 Soil and root depth impact on evapotranspiration

Hypothesis: Transpiration is reduced by reducing the root or soil depth.

Site: OBS

Time period considered: January 1, 2001 to December 1, 2001

By default, CLASS the three layer depths in the model runs were set to 0.1, 0.25, and 3.75 m. The third layer can be sub-divided into several layers with the desired thickness. In this experiment, we first perform model runs by altering the third soil layer depths to 1.25, 1.75, 2.0, 2.5, 3.0, and 4.15 m. Next, we explore the sensitivity of root depth by changing the rooting-depth parameter to 0.08, 0.15, 0.20, 1.0, and 2.0m. All the parameters remain the same as the baseline run except for the root or soil depth. The effects of different soil and root depths on soil evaporation and transpiration fluxes are quantified by looking at the cumulative evaporation and transpiration for a whole year.

4.5.3 Soil moisture impact on ET

Hypothesis: Increase in soil moisture increases the ET.

Time period considered: June 14, 2008 to July 1, 2008

Site: OJP

In this experiment, as a preliminary exercise before looking at the impact of ice content, we investigated the impacts of liquid soil moisture on ET in ice- free conditions. The site selection for this experiment was based on the fact that OJP has the simplest configuration for the soil layers among the three sites. OBS and OAS have organic soil layer which modifies the soil properties. The soil moisture was controlled by adjusting the initial condition, which was set to volumetric water contents of: 0.1, 0.15, 0.18, 0.2, 0.25, 0.3, 0.35, and 0.4 (uniform in all soil layers). All the parameters remain the same as the baseline run except for the liquid water content. The impact of soil moisture on cumulative bare soil evaporation, cumulative transpiration, cumulative partitioning of ET, total transpiration, and partitioning of total transpiration between the three soil layers and water stress is studied. Water stress (K_c), scaled roughly from 0 (severe stress) to 1 (no stress), is calculated from equation 29 below.

$$K_c = \frac{AET}{PET} \tag{29}$$

where AET is actual ET (simulated total ET from CLASS) and PET is for a well-watered grass reference surface, which was applied at a daily time scale and was calculated by the Food and Agriculture Organization (FAO) Penman-Monteith equation as follows (Allen et al., 1998):

$$PET = \frac{0.408\,\Delta\,(R_n - G) + \gamma \frac{900}{T + 273} u_2 (e_s - e_a)}{\Delta + \gamma(1 + 0.34u_2)} \tag{30}$$

where R_n (Wm^{-2}) is net radiation at surface , G (Wm^{-2}) is soil heat flux, T $(°C)$ is mean air temperature, u_2 is (m/s), $e_s(kPa)$ is saturation vapor pressure, e_a $\left(\frac{kPa}{°C}\right)$ is actual vapor pressure, Δ $\left(\frac{kPa}{°C}\right)$ is slope of saturation vapor pressure curve, and γ $\left(\frac{kPa}{°C}\right)$ is psychrometric constant.

4.5.4 Frozen soil moisture impact on ET

Hypothesis: Unknown

Time: October 1, 1999 to January 1, 2012

Site: OJP

This experiment considered the role of the soil freezing and thawing process for plant water uptake and simulation of ET. This process in the real world is poorly understood. Moreover, the outcome in the model was likely to be an emergent feature of a series of assumptions, rather than something parameterized directly. As a result, we did not know what to expect from this experiment. For this experiment, we did not re-run the model but rather analyzed the relationships between the output of variables from the baseline run. The variables examined were VWC-liquid, VWC-ice, soil temperature and transpiration, which were taken from layer 1, since this layer froze the most.

4.6 Model calibration, validation, and uncertainty analysis

For our calibration, the Monte Carlo-based generalized likelihood uncertainty estimation (GLUE) method was applied for each site with 10,000 realizations and a new set of randomized vegetation and soil hydraulic properties was sampled for each model run from the selected parameter ranges in Table 7 (Beven and Binley, 1992). The calibration study does not use the pedotransfer function as it constrains the model parameters and underestimates the uncertainty in the fluxes (Ireson et al., 2021). In the calibration study, the four hydraulic properties (θ_p, b, ψ_s, K_s) were sampled

directly rather than using the pedotransfer functions that sample X_S (%) and X_C (%). Nazarbaskh et al. (2020) reported that the minimum and maximum LAI, L_{min} and L_{max} (-), the minimum stomatal conductance, $r_{s,min}$ (s/m) and a drainage index, ϕ (-) strongly affect the hydrological fluxes in CLASS. Therefore, these parameters were sampled along with four hydraulic parameters in the calibration. In order to ensure that $L_{min} \leq L_{max}$, a f_L factor is added to the calibration that ranges from 0.5-1.25. L_{min} is the minimum of (L_{max}, $L_{max}f_L$). The data quality check followed the method in Ireson et al. (2021).

Table 7: Parameter range of the Monte Carlo calibration for CLASS for OJP, OBS, and OAS

Parameters	Unit	OJP	OBS	OA
θ_p	(m^3/m^{-3})	$0.1 - 0.4$	$0.2 - 0.7$	$0.2 - 0.5$
b	-	$3 - 18$	$3 - 18$	$3 - 18$
ψ_s	(m)	$0.05 - 3$	$0.05 - 3$	$0.05 - 3$
K_s	(m/s)	$10^{-7} - 10^{-4}$	$10^{-7} - 10^{-4}$	$10^{-7} - 10^{-4}$
ϕ	(-)	$0 - 1$	$0 - 1$	$0 - 1$
L_{max}	(-)	$2 - 4$	$2 - 4$	$1 - 4$
f_L	(-)	$0.5 - 1.25$	$0.5 - 1.25$	$0.5 - 1.25$
$r_{s,min}$	(s/m)	$50 - 300$	$50 - 300$	$50 - 300$

A total of eight parameters were sampled in this study. Choosing a suitable parameter range has included measured values, experiments, literature values, and expert judgement (Ireson et al., 2021; Bartlett et al., 2003). The three layer depths in the model runs were set to 0.1, 0.25, and 1.6 m.

For the calibration, the models were run for all three sites at an hourly timestep from August 1, 2013 and ends on September 30, 2015 due to the computational expenses of running 10,000 runs. The performance of a model run to predict observation is represented by objective functions,

and the choice is often subjective (Beven and Binley, 1992). Here, the performance of each model run is determined by calculating the root mean square error (RMSE) of the ET and cumulative change in liquid water content for each depth. We conducted a single objective (ET) and multi-objective (soil moisture and ET) calibration for 10,000 model runs. A detailed explanation of the use of the objective function is presented below.

4.6.1 Single objective function

To perform the single objective calibration, we first calculated RMSE of the daily ET fluxes (calculated using the scikit-learn Python package; Pedregosa et al., 2011)

$$\mathrm{RMSE}_{\mathrm{ET}} = \sqrt{\frac{\sum_{i=1}^{n}(\Theta_o - \Theta_s)^2}{n}} \tag{31}$$

where Θ_o and Θ_s are the daily ET fluxes from the observations from the flux towers and simulations from the Monte Carlo runs, at time index I, and n is the number of points in time.

The 30 lowest RMSE were identified as 30 behavioral model runs, as well as the single best performing realization.

4.6.2 Combined objective function

It is possible to combine the two single objective functions and get a combined objective function (COF) using the normalized RMSE of soil moisture and ET. For the second single objective function, we calculated the RMSE of the cumulative change in liquid water content for each depth and then averaged it over the three layers, as in the equation below:

$$\epsilon_j = \sqrt{\frac{\sum_{i=1}^{n}\left(\Theta_{o(i,j)} - \Theta_{s(i,j)}\right)^2}{n}} \tag{32}$$

$$\mathrm{RMSE_{SM}} = \sum_{j=1}^{3} \frac{\epsilon_j}{3}$$

where $\Theta_{o(i,j)}$ and $\Theta_{s(i,j)}$ are the cumulative change in VWC-liquid from the observations at the three sites and simulations from the Monte Carlo runs, respectively and depth index j, and $\mathrm{RMSE_{SM}}$ is the overall performance metric, with units of VWC (m^3/m^3).

$$\mathrm{COF} = \sqrt[2]{(\mathrm{NRMSE_{SM}})^2 + (\mathrm{NRMSE_{ET}})^2} \tag{33}$$

where,

$$\mathrm{NRMSE_{ET}} = \frac{\mathrm{RMSE_{ET}}}{\mathrm{maximum(RMSE_{ET})}}$$

$$\mathrm{NRMSE_{SM}} = \frac{\mathrm{RMSE_{SM}}}{\mathrm{maximum(RMSE_{SM})}}$$

COF represents the Euclidean distance to the optimum solution, and parameter sets with the 30 shortest Euclidean distance considered the best performing realizations. The goal was to find a combination of the parameters that minimizes RMSE for ET without significant performance degradation of cumulative change in liquid water content. The expectation from this multi-objective function calibration was to reduce the total uncertainty in infiltration, drainage, and runoff compared to single objective calibration.

The validation period started on August 1, 1999 and ended on July 30, 2013. The validation run consisted of 30 behavioral realizations. The ET and soil moisture simulation with observations were evaluated to explore the uncertainty in fluxes and states of the runs. Daily simulated ET was compared against the observed ET to explore the performance on a weekly as well as an annual basis. The simulated cumulative change in liquid water content was compared with the observed data.

From the 30 best performing realizations, the spread in the annual simulated fluxes were calculated as a measure of total uncertainty. The difference between the maximum and minimum data points at the end of the hydrological year is the total uncertainty. The performance in uncertainty is compared for single-objective calibration and multi-objective calibration.

5 Results and discussion

5.1 Baseline model runs

In the baseline run, we ran CLASS with standard configurations, i.e., default vegetation and soil parameters and made sure the vegetation reflected the right PFTs (Plant Functional Type) for the individual sites (Figure 4). The annual water balances were successfully closed using the fluxes and states from the model output as the sum of change in storage, ET and runoff and drainage is equal to the infiltration. The annual water balance shows that the infiltration and ET are significantly higher in OA compared to OBS and OJP. Simulated ET in CLASS is composed of the following components: transpiration from the three soil layers, soil evaporation, water vapor flux from liquid water on vegetation, water vapor flux from ice on vegetation, and water vapor flux from snowpack. In all three sites, ET takes a steep rise in spring following the snowmelt and peaks at summer and the seasonal variation of ET agreed well with the observations. The model results show that CLASS performed well in simulating the onset of spring ET and that ET is overestimated in the spring and early summer at all three sites.

Transpiration is the single largest component of ET at all three sites (Table 8). However, the proportion of T relative to ET at each site varies: it is highest at OA due to the vegetation, which is a deciduous broadleaf site with higher transpiration rates than the evergreen conifers; it is lowest at OBS, due to the organic soil layer at this site which results in higher bare soil evaporation compared with the mineral soils at OJP. The scientific community has paid particular attention to the partitioning of ET (Chang et al., 2018). ET components can respond greatly to changes in vegetation and environmental conditions, but the two major components of ET are transpiration and soil evaporation (Zhang et al., 2016).

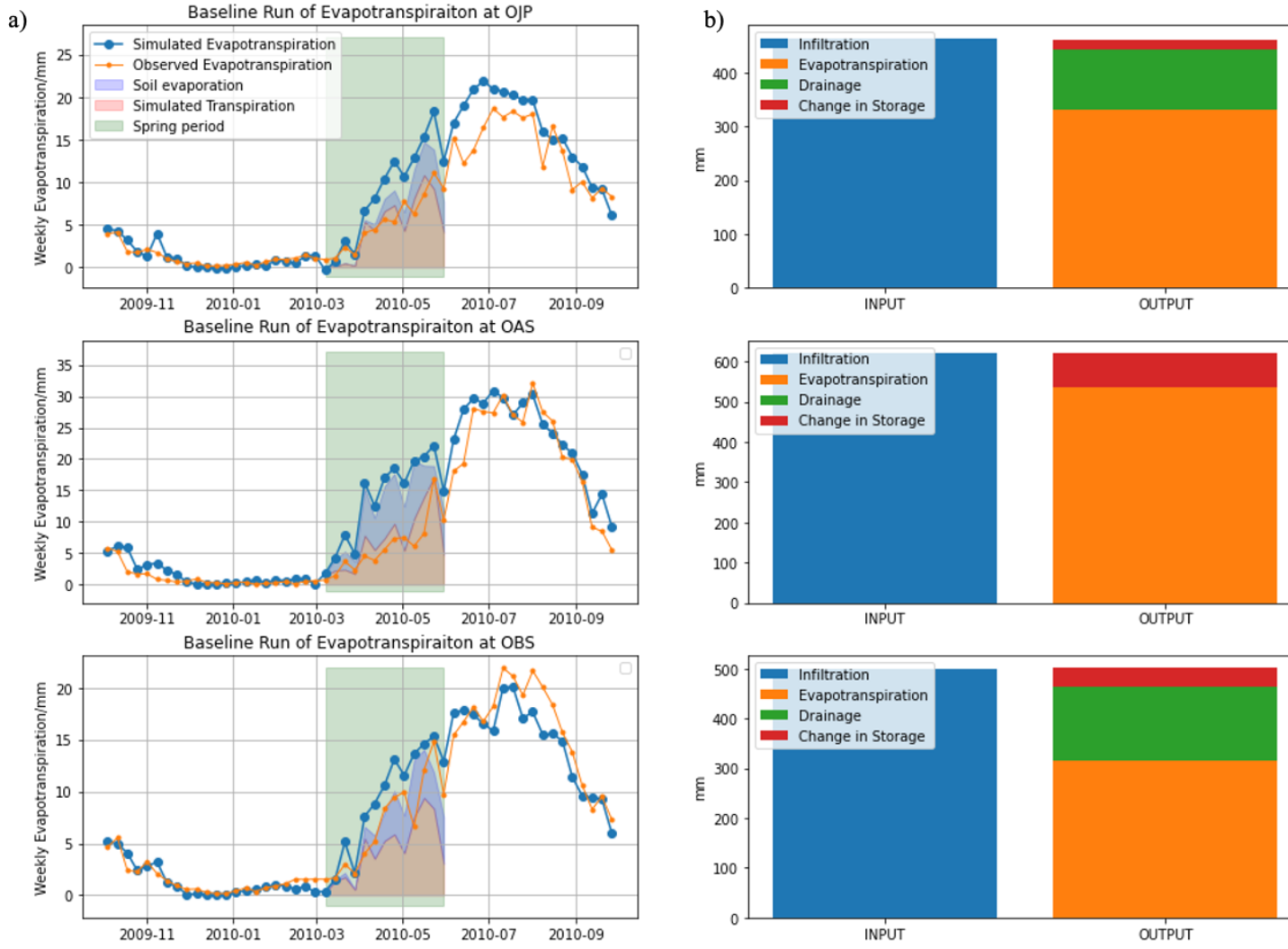

Figure 4: a) Comparison between CLASS baseline run of simulated total ET and observed ET for the three boreal forest sites OJP, OBS and OA for October 1st 2009 – September 30th 2010. The orange solid line represents the observed total ET, the blue solid line represents the simulated total ET (which includes canopy evaporation/sublimation and snowpack sublimation). The shaded green area represents the melt period. The red shaded area represents the simulated transpiration component of total ET, and the blue shaded area represents the simulated bare soil evaporation of total ET. b) the yearly water balance components of the CLASS model for the period of simulation are successfully closed

Previous studies have shown CLASS overestimated ET in the spring period at OJP, which is consistent with other studies using different models (Nazarbakhsh et al., 2020). These results at other sites (OBS and OA), alongside other simulations in the literature (Nazarbakhsh et al., 2020), suggest that this may be a generic issue in seasonally frozen soils. Studies on ET partitioning have shown that the transpiration ratio is high in densely vegetated, and water limited areas (Scot et al., 2006; Cavanaugh et al., 2011). Boreal forest soils often have a thick upper organic layer that changes the soil hydrological and thermal regimes (Mölders and Romanovsky, 2006; Lawrence and Slater, 2008). Soil evaporation is mainly impacted by the properties of the shallow soil layers, whereas transpiration is affected by the deeper soil layers (Sun and Verseghy, 2019). Radforth and Brawner (1977) stated that porosity of organic soil rarely goes below 0.8 whereas the porosity of mineral soil layer is around 0.4 (Dingman,1994). A peaty soil layer has more porosity and can hold more water, thus simulated soil evaporation in CLASS at a peaty soil is higher than a mineral soil. Among the three sites, the largest difference between observed and simulated ET is seen at OA. CLASS seems to overestimate transpiration more in broadleaf compared to conifers.

Table 8:Average simulated and observed ET for spring period (1st March- 30th May) from 2000 to 2015

	OJP	OBS	OA
Simulated transpiration (mm)	59.6	50.1	84.3
Transpiration/ET (%)	56.4	49.5	57.0
Simulated soil evaporation (mm)	24.5	27.4	45.0
Bare soil evaporation/ET (%)	23.2	27.0	30.0
Canopy evaporation (mm)	21.2	23.2	15.7
Total simulated ET (mm)	105	101	146
Total observed ET (mm)	56.9	75.9	57.7

5.2 Numerical Experiments

5.2.1 Infiltration into frozen and unfrozen soil

In this numerical experiment, we investigate how the liquid water content and ice content of the first soil layer impact the infiltration process in CLASS. Our expectation is that, in the absence of macropores (which are not represented in CLASS), there should be no infiltration if the first soil layer is frozen and saturated. The model predicted that infiltration occurred while the first soil layer was still frozen and saturated (Figure 5a). The change in amount of soil water storage in layer 1 and layer 3 remains constant but we saw an increase in layer 2. The infiltration experiment showed that in the model infiltrated water can bypass the first layer to enter the second, even when the first layer is frozen and saturated. Even though this behaviour seems erroneous and unexpected, it may in fact act as a way to replicate the infiltration into frozen soils with preferential pathways, e.g., macropores and cracks, and hence give better model performance compared with a model where there is no infiltration. Stadler et al. (2000) in their frozen soil experiments showed that infiltration and percolation in frozen soil can occur through macropores. Demand et al. (2019) concluded from their study that macropores in soil with a thin seasonally frozen soil layer (8-25 cm) at saturation can retain an infiltration capacity of around an order of magnitude higher than the calculated matrix infiltration rate.

32 different simulated infiltration runs under various precipitation intensity, soil water content, and ice content, sandy and clayey soil (Table 6) were considered. Each data point in the scatter plots (Figure 5b and 5c) of actual infiltration vs potential infiltration represents a model run from one of the 32 combinations. It is interesting to note that infiltration does not completely shut down even if both the first and second soil layers are frozen and saturated. We can see from Figure 5b and Figure 5c that for the same potential infiltration, there is more runoff and less infiltration as

we increase the soil layers that are saturated and frozen. The black solid line in Figure 5b and 5c shows that even when all three soil layers are frozen and saturated, a small amount of water still infiltrates. Soil texture (percentage of sand, silt, and clay) is one of the major factors affecting the infiltration capacity. In the absence of ice in the soil layers, we can see that almost all the water infiltrates in a sandy soil because of the large pores. However, in a clayey soil we see that infiltration amount reaches to a maximum at around 250 mm because it has smaller pores and less permeability.

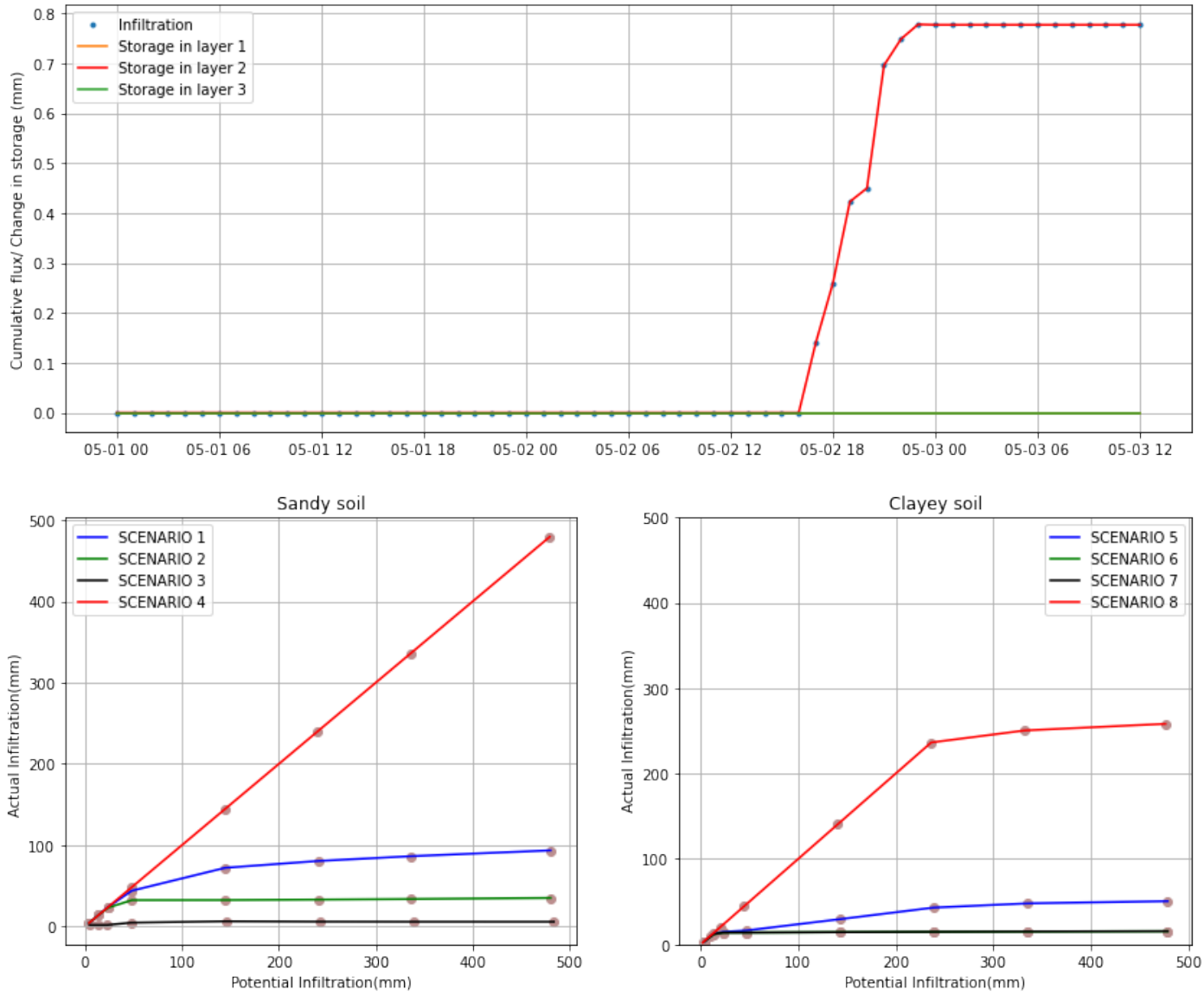

Figure 5: Top panel: Water content (Storage) of layer 1, 2 and 3 after infiltration in a frozen and saturated first layer. The red line shows the increase in storage and the blue dots shows the infiltrated water. The orange and green line stay constant. Bottom left panel: Simulated cumulative infiltration of the CLASS model according to potential infiltration as influenced by ice content and liquid content in a sandy soil. Bottom right panel: Simulated cumulative infiltration of the CLASS model according to potential infiltration as influenced by ice content and liquid content in a clayey soil. The scenarios are explained in the Table 6 in the methods section.

5.2.2 Soil and root depth impact on the ET

In this experiment, the soil depth or root depth was reduced, with the expectation that doing so would reduce transpiration. Total transpiration increased with increased root depth to a maximum amount that is achieved when the roots are 1.0 deep or deeper (Figure 6). When the root depth is less than the thickness of the first soil layer (i.e., a root depth of 0.08 m in Figure 6), the atmospheric demand for transpiration is only able to draw on water within the first soil layer. When the root depth extends into the third layer, (i.e., a root depth of > 0.35 m), the atmospheric demand for transpiration can draw on moisture from all three soil layers. Consequently, we see the transpiration in the first soil layer to be highest for the vegetation with the shortest root length and lowest for the longest root length. However, the limited water available to extract from the first soil layer cannot completely fill the demand for overall transpiration. So overall transpiration of root depth 0.08m is less as compared to that of root depth 1m. As the rooting depth increases, the root has access to more soil moisture from deeper soil layers.

Figure 7 illustrates the impact of soil depth on ET in CLASS. We can see from the figure that the total transpiration is same irrespective of the total soil depth. However, the contribution for total transpiration from each soil layer was different depending on the soil layer configuration (Figure 7). A decrease in soil depth from third soil layer decreases the available soil moisture for transpiration. Thus, the transpiration demand is mainly filled by the first and second soil layer. Transpiration with 1.5 m soil depth was the highest in layer 1 and layer 2 and the least in the layer 3. On the other hand, transpiration with 4.0 m soil depth was the least in layer 1 and layer 2 and the highest in layer 3. In order to fill the transpiration demand, water losses from layer 1 due to transpiration is greater in 1.5 m soil depth compared to 4.0 m.

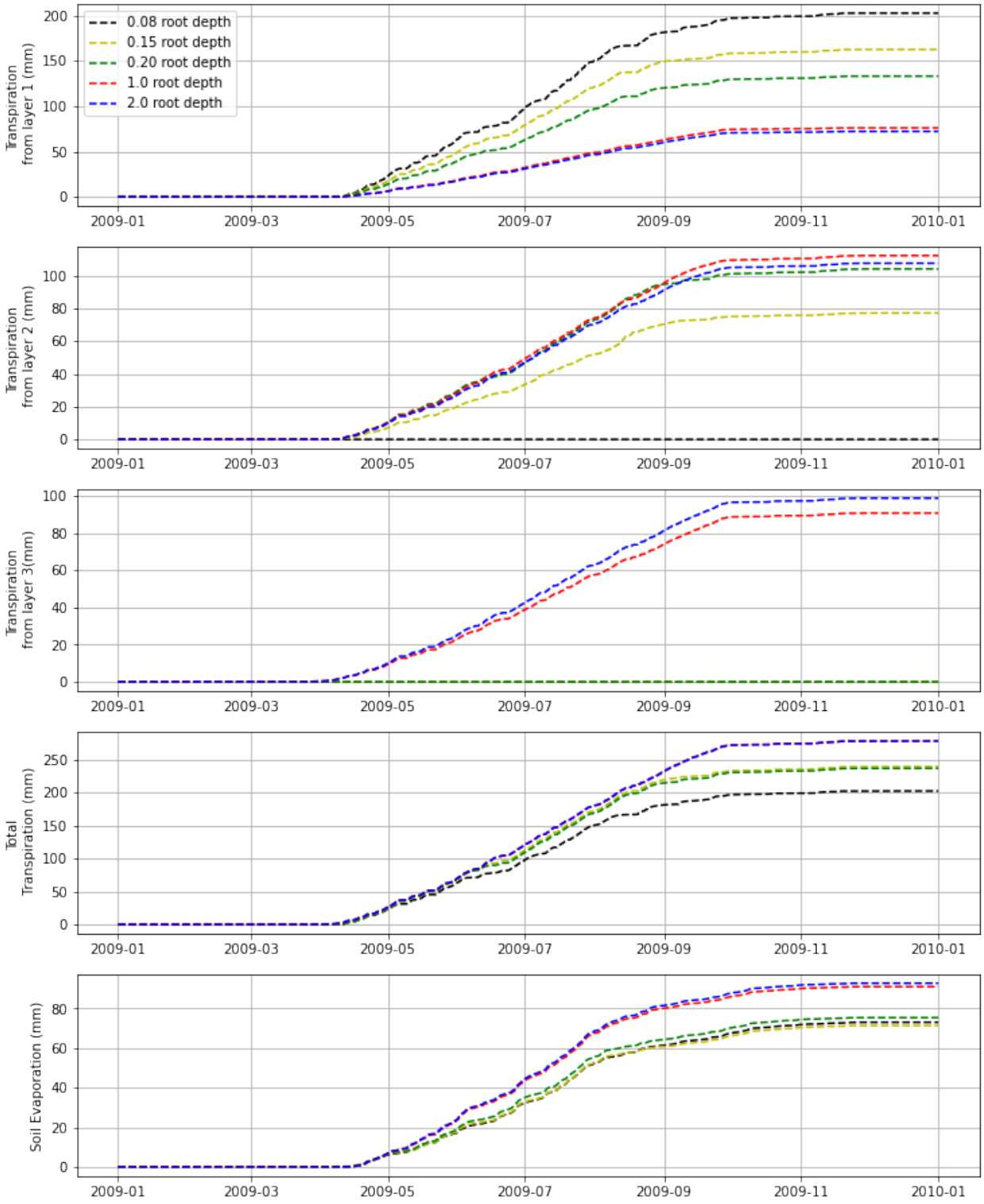

Figure 6: Transpiration and soil evaporation response to changing root depth in the CLASS simulation. The black, yellow, green, red and blue dotted line represent the model run with 0.08 m, 0.15 m, 0.2 m, 1.0m and 2.0m root depth at OJP respectively.

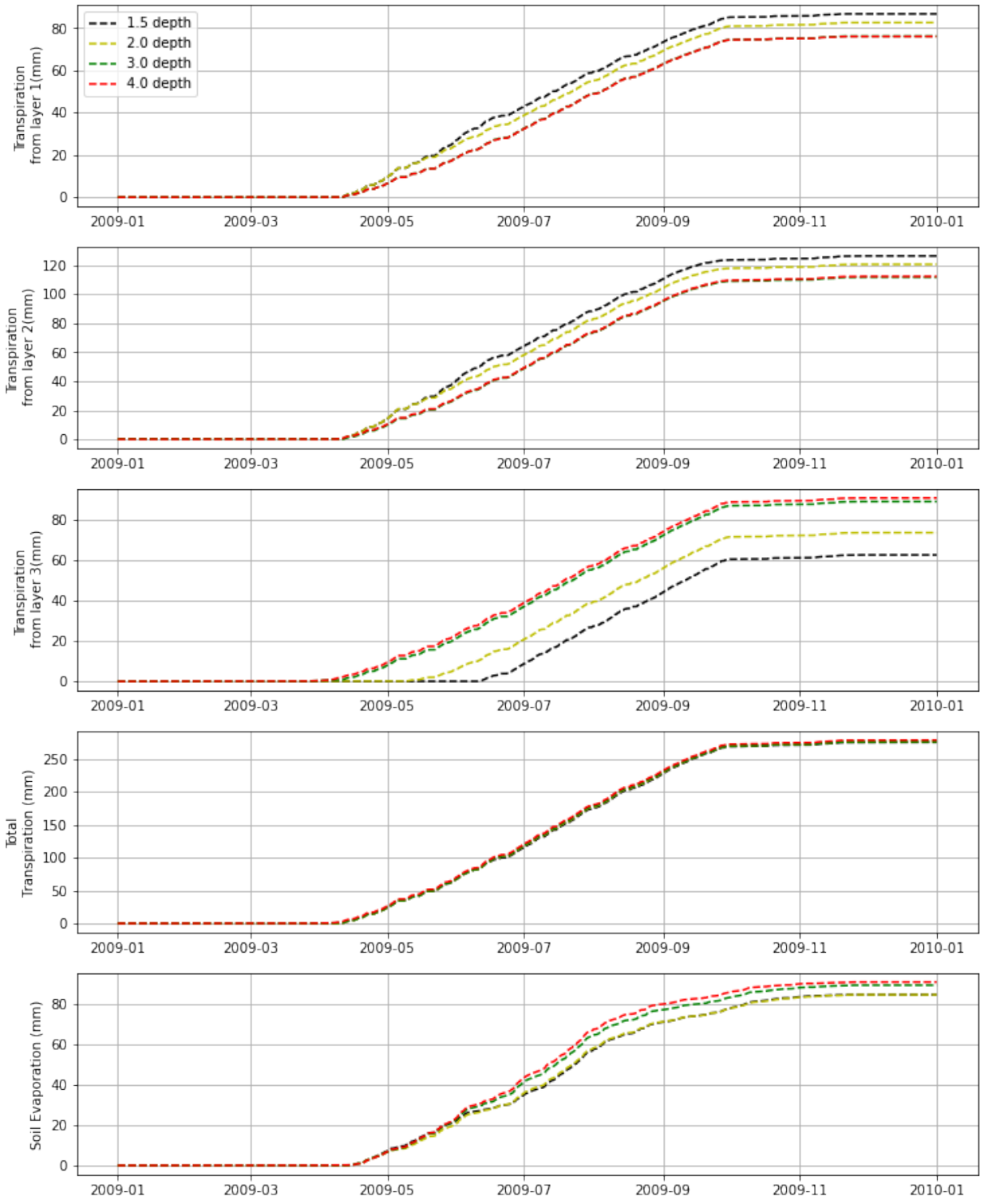

Figure 7: Transpiration and soil evaporation response to changing soil depth in the CLASS simulation. The black, yellow, green, and red dashed line represent the model run with 1.5 m, 2.0 m, 3.0m and 4.0m third soil layer depth at OJP respectively.

So, there is less soil moisture available for evaporation at 1.5 m soil depth. Thus, cumulative bare soil evaporation is highest at soil depth of 4.0m and lowest at 1.5m.

Chen et al. (2018) reported that increased soil depth in the VIC model had an impact on the water and energy simulations and that the simulated annual ET was much higher because more water was available for soil evaporation. He also stated that it was important to include soil depth in the calibration of land surface models. The finding from this experiment suggests that simulated ET in CLASS is not significantly impacted by changing the soil depth in the model. On the contrary, we found that soil root depth impacted the simulated ET in CLASS. Liu et al. (2020) showed in his study that a shorter root depth limits the soil moisture availability and ultimately ET and that incorporating a dynamic rooting depth in LSMs improves both soil moisture and ET simulation.

5.2.3 Soil moisture impacts on ET

ET can be supply-limited, or energy limited (Koster et al., 2004; Seneviratne et al., 2006; Teuling et al., 2009). ET is independent of soil water content in the energy-limited conditions. Soil moisture can be below wilting point or between critical water content and wilting point in supply-limited ET. Soil moisture can restrict ET between wilting point and critical water content. In this experiment, we examine the impact of soil moisture on evaporation and transpiration.

There is no significant change in the transpiration with water content when the VWC-liquid is ≥ 0.2 (Figure 8). As long as VWC-liquid is sufficient to meet the energy-limited transpiration demand, transpiration occurs at a maximum rate. As VWC-liquid falls below 0.2, transpiration reduces in a roughly linear relationship with reducing VWC-liquid. At very low levels of VWC-liquid, plants reach a threshold in CLASS where soil transpiration is turned off because the suction is high enough that plant roots cannot extract water from soil. On the other hand, soil evaporation

is heavily influenced by the available VWC-liquid in the first layer and does not seem to have any thresholds. We see the evaporation happening, even when transpiration is turned off at low VWC-liquid. The evaporation starts to increase as the VWC liquid increases. In this numerical experiment, we increase liquid content to 0.4. However, in CLASS the fibric peat parametrization can allow VWC-liquid to go as high as 0.93 (Verseghy et al., 2012). Thus, by adding an organic soil in the first layer, water available for bare soil evaporation increases. This explains the higher rates of soil evaporation at OBS and OA which both have an organic soil layer at the surface.

At 0.1 VWC-liquid, evaporation is the largest component of the ET partitioning (i.e 100% at 0.1) (Figure 8). As the VWC-liquid increases from 0.1 to 0.2, evaporation starts to form a smaller percentage of total ET. At around 0.2 VWC-liquid, evaporation only forms about 11.2% of the total ET which makes transpiration the dominant component. An increase in VWC-liquid after 0.2 does not increase the transpiration amount but increased the amount of evaporation as seen in Figure 8a. Thus, an increase in VWC-liquid from 0.2 to 0.4 increased the soil evaporation partitioning from 11.2% to 32.4%.

Another interesting observation is that when water is limited, ET is supplied from deeper soil layers as seen in Figure 8b. For instance, at 0.15 VWC-liquid, transpiration from layer 1 forms a relatively small portion of total transpiration. However, when there no restrictions of moisture levels, transpiration is drawn from soil layers according to the relative fraction of roots in each layer in CLASS (Equation 42, Sun and Verseghy, 2019).

$$R(\Delta z) = \frac{e^{-3z_t} - e^{-3z_B}}{1 - e^{-3z_r}} \tag{34}$$

where z_t is the depth of the soil layer top, z_B is the depth of the soil layer bottom and z_r is the overall rooting depth.

Using 4.1 m overall rooting depth in CLASS, $R(\Delta z)$, the root fractions for the three active soil layer depths 0.10, 0.25 and 3.75 m, are 0.26, 0.39 and 0.35 respectively. We can see that the second soil layer constitutes the major fraction of the total root and thus forms the most dominant component of the total transpiration. Thus, when we increase soil liquid content from 0.25 to 0.4 transpiration from layer 2 is the most dominant component of total transpiration.

In the above experiments, we have only considered the impact of soil moisture on evaporation and transpiration. The water stress function, defined as the ratio of total ET from the model over PET from the Penman Monteith equation, includes all components of ET (Figure 8). Note that the water stress can be greater than 1 because the parameters in the Penman Monteith calculation differ from those in the more complex and more comprehensive CLASS model. We can see there is no water stress when the water content is 0.35 or greater. There is a small linear decline in water stress between water contents of 0.35 down to 0.2, as soil evaporation reduces. Below 0.2 there is a rapid drop in water stress (corresponding to less ET) due to the reduction in transpiration.

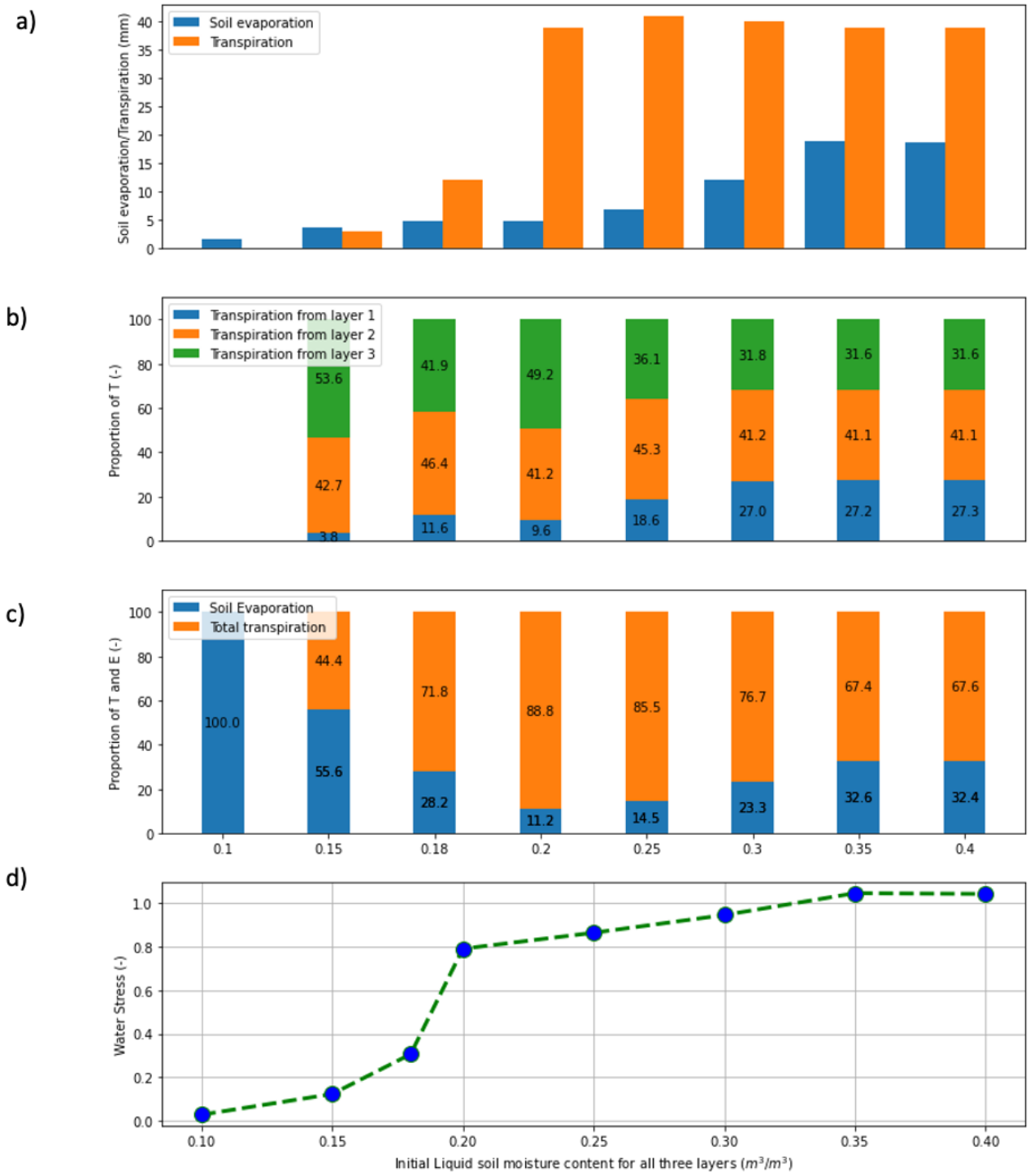

Figure 8: The sensitivity of a) total E and T, b) proportion of the T originating in different soil layers, c) proportion of T and E and d) water stress to liquid soil moisture water content (uniform in all soil layers) at OJP from July 14, 2008 to August 1, 2008.

5.2.4 Frozen soil moisture impact on ET

In this experiment we explore how frozen soil impacts transpiration in CLASS. This shows that there is only VWC-liquid when the temperature is greater than or equal to 0^0C (Figure 9). However, in real soils the freezing point of soil water is depressed below 0^0C (He et al., 2016), the phenomenon of freezing point depression, which is due to a combination of solute effects and capillary/adsorption effects in the soil, and is characterised by the SFC (Amankwah et al., 2021). This means that the upper limit of VWC-liquid declines gradually as the temperature declines below 0℃. CLASS does not take freezing point depression into account. The lack of representation of freezing point depression in the model results in soil temperature staying at 0℃ for a long time until all ice is turned into liquid and means that ice and liquid can coexists in the pore space, but only while the soil is at 0℃.

Soil temperature is acting as a step function for transpiration (Figure 9), where transpiration is turned off in the model when soil temperature is less than 0℃. The results show that water stress impacts transpiration for the processes of drying (unfrozen soils) and freezing (frozen soils) (Figure 9). During drying, liquid water content is replaced by air and during freezing liquid water content becomes ice content. In both cases, transpiration is shut down at low liquid water content values. Transpiration increases for liquid water contents above 0.07 but the rise is sharper in the unfrozen soil compared to frozen soil. So, the transpiration behavior appears slightly different for a drying and freezing soil. In Figure 9d transpiration is plotted as a function of ice content, for frozen and unfrozen soils.

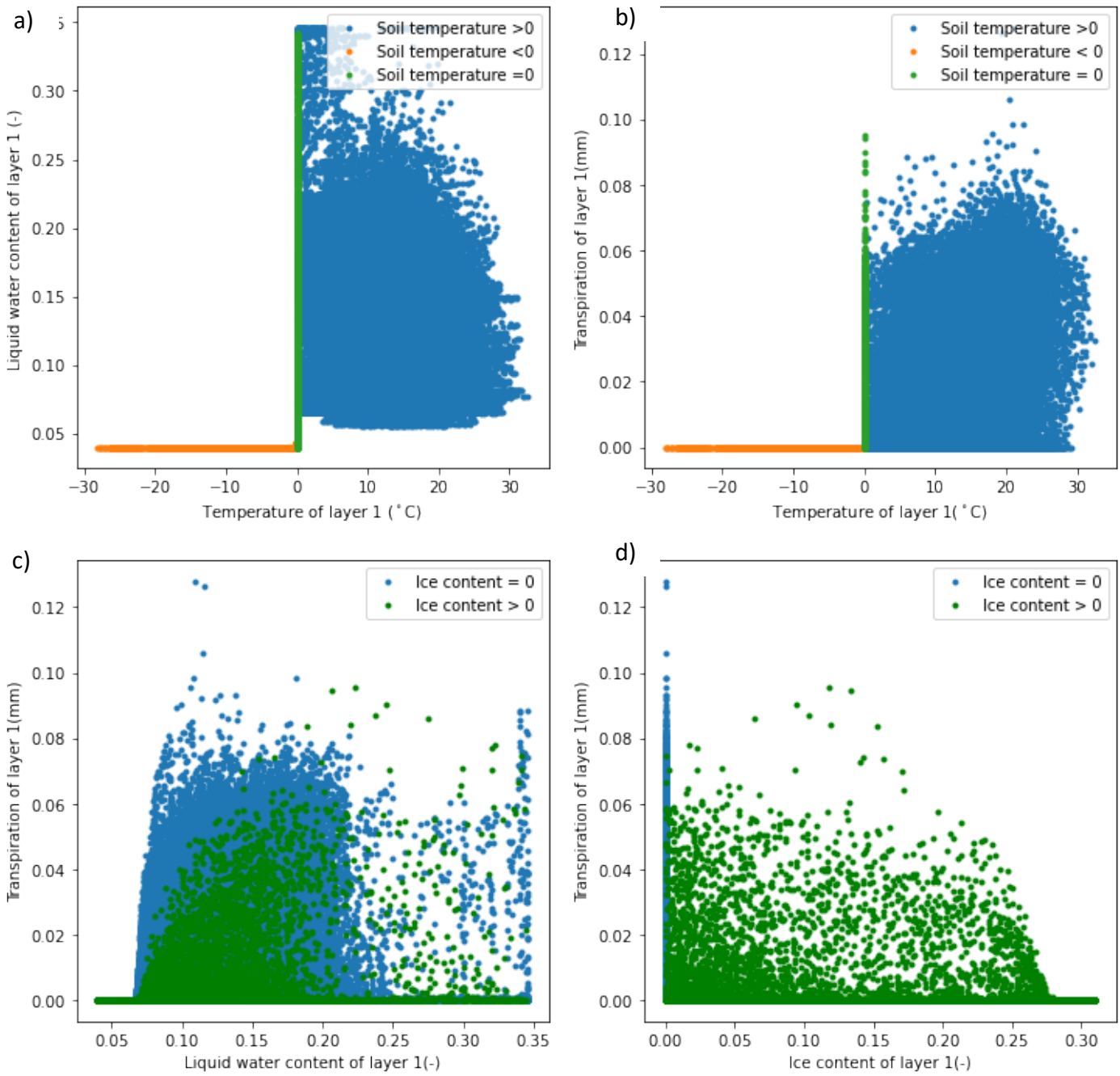

Figure 9: Plots of the relationships between different variables for soil layer 1, output by CLASS: (a) the Soil Freezing Characteristic curve (b) Transpiration of layer 1 dependence on temperature of soil layer 1 (c) Transpiration of layer 1 dependence on liquid water content in unfrozen and frozen condition (d) transpiration of layer 1 dependence on ice content at OJP. The points in the plot represent the baseline CLASS hourly model output at OJP (1999-2011).

This again shows that transpiration is shut down when ice completely displaces liquid water content. The behaviour that can be deduced from Figure 9 reveals a significant model deficiency, which is the absence of a freezing point depression. If freezing point depression were included in the model, the soil temperature would drop below 0℃ during the phase transition from liquid to ice. Since transpiration appears to be dependent on the remaining liquid water content during freezing, transpiration is expected to be occurring below 0℃ . It can be speculated that transpiration should not occur at soil temperatures below 0℃ , even if liquid water remains in a supercooled state in the soil pores. That being the case, two modifications are recommended to the model: 1) inclusion of freezing point depression, and 2) modification of the water stress function such that no transpiration can occur below 0℃ .

We are unable to make the above modifications in this study. However, we can speculate about the effect of doing so. To do this, simulated transpiration at OBS is partitioned for each soil layer into three periods: one where simulated soil temperature is less than 0℃ , one where simulated soil temperature is equal to 0℃ and one where simulated soil temperature is greater than 0℃ , as shown in Figure 10. Figure 10 shows again that no transpiration occurs when the temperature is less than 0℃ , but that a significant proportion of transpiration is happening when the soil temperature is equal to 0℃ in all the soil layers. When transpiration at 0℃ is subtracted from the simulated total ET, there is a big improvement in the simulation of ET during the melt period, compared with the flux tower data. This suggests that the problem of over-estimation of spring ET in the model could potentially be attributed to limitations with plant water uptake from frozen soils and can be addressed by the proposed modifications. Wu et al. (2018) noted that implementing freezing point depression function in CoupModel significantly improved the simulated soil temperature and total water content in two seasonally frozen soils in northern China.

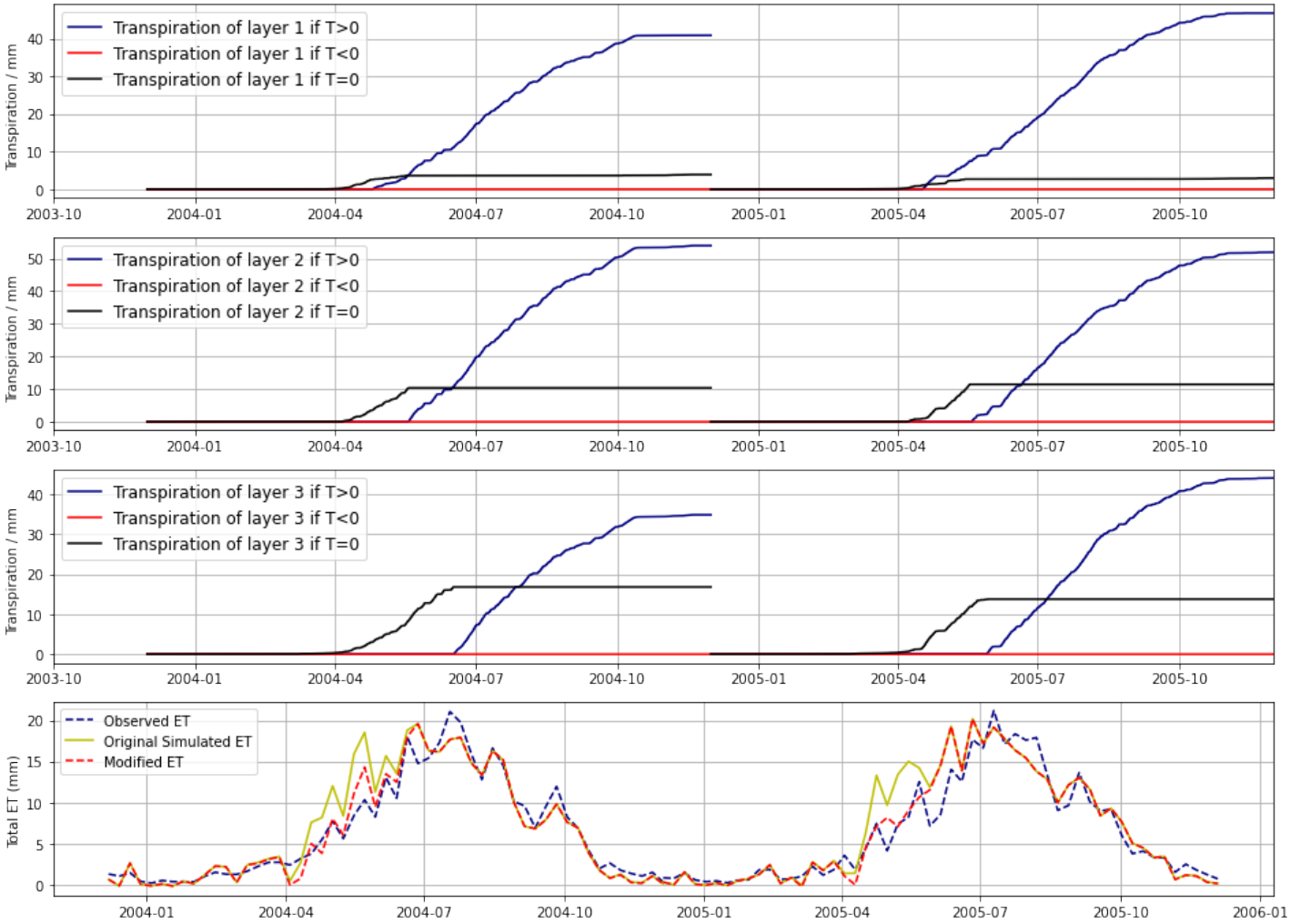

Figure 10: Cumulative simulated transpiration from each soil layer at different soil temperatures. The blue solid line represents the simulated transpiration when soil temperature is greater than 0. The black solid line represents the simulated transpiration when soil temperature is equal to 0. The red solid line represents the simulated transpiration when soil temperature is less than 0. The blue dashed line represents the weekly observed ET at OBS. The yellow solid line represents the weekly baseline run of ET at OBS. The red dashed line represents the modified weekly ET at OBS.

Mellander et al. (2004) conducted a study at young Scot pine stand in the boreal zone of northern Sweden and reported that the presence of liquid water alone was not enough to initiate transpiration. It was also important to consider the low soil temperature in the soil layers. Low temperature restricts photosynthesis by limiting mobility in roots and water supply and ultimately stomatal closure (Woodward and Kelly, 1997). Furthermore, Mellander et al. (2006) demonstrated that if models don't account for the influence of low soil temperatures on stomatal conductance, there is the potential for overestimation of transpiration.

5.3 Model Calibration, validation and uncertainty analysis

We now explore the capability of the CLASS model for predicting ET when the model parameters are calibrated. First, we look at the single objective calibration where daily observed ET from flux towers at OJP, OBS and OAS is used for calibration. The simulated total ET from the baseline run and the behavioral realizations were compared with the above canopy estimates from eddy correlation flux towers (Figures 11–13). The model results show that calibration has improved the ET simulation, but we still see that the spring ET is overpredicted in many years (calibration and validation periods). Looking at the cumulative yearly ET at the three sites, the simulated ET at the end of the hydrological year seems to be predicted reasonably well for OJP, OBS and OA (Figure 14). Most of the observed ET at the end of hydrological year falls within the uncertainty range of behavioral realizations.

Focusing on the single run for each site with the lowest RMSE among the behavioral realization, we compare the performance for the baseline run and calibration period. At OJP, the RMSE of the baseline ET run was 0.7 mm/day. For the calibration period, the RMSE and R^2 value for OJP were 0.64 and 0.90, respectively. Similarly, at OBS, the RMSE of baseline ET run was 0.45

mm/day. The RMSE and R^2 value for the calibration period were 0.43 and 0.86 respectively. Likewise, at OA, the RMSE of baseline ET run was 1.20 mm/day. For the calibration period, the RMSE and R^2 value for OJP were 0.73 and 0.81 respectively.

The RMSE and R^2 values during the validation period were 0.60 and 0.88 respectively at OJP, 0.41 and 0.84 at OBS, and 0.67 and 0.82 at OA. Surprisingly, the RMSE values were marginally better during the validation period in comparison to the calibration period. Like in the baseline runs, the performance at OJP and OBS (coniferous forest) is significantly better than OA (broadleaf deciduous forest); however, we still see some overestimation of ET during the spring at all sites in some years. Overall, the observed data were closer to the behavioral model runs than the baseline runs at OJP and OA for most years. The performance at OBS does not alter much after calibration. Looking at the annual ET, we can also see improvement at OA and OJP where the baseline run mostly overpredicts annual ET (Figure 14), and the uncertainty is higher for higher ET values (Figures 11–13). Some researchers (Vrugt et al., 2008; Houska et al., 2014) have suggested that the GLUE method overestimates the uncertainty in high events in hydrological model simulation. The uncertainty bounds could be further reduced by doing more model runs and setting a stricter threshold, however, the run time becomes computationally expensive.

Next, we look at the uncertainty in all simulated fluxes when observations of ET are used to constrain the model. Here, we considered the 30 best realizations and noted the spread in the annual fluxes as a measure of total uncertainty. The total uncertainty was derived by calculating the difference between the maximum and minimum data points at the end of each hydrological year which yielded 15 total uncertainty values for each fluxes (i.e. Drainage, Infiltration, Runoff, ET) . Then, the median was calculated for those 15 total uncertainty values that is shown in Table 9.

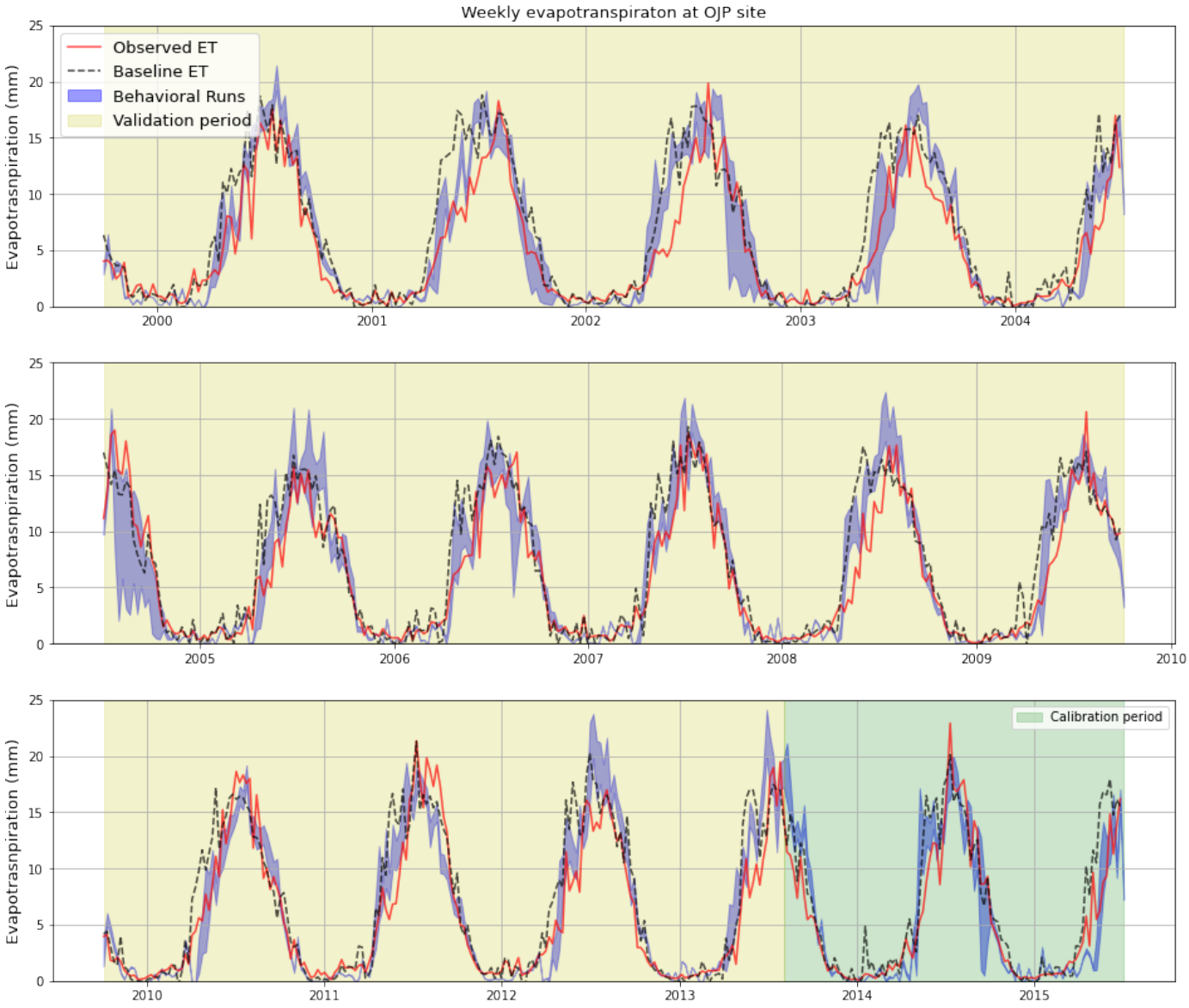

Figure 11: OJP model validation (1999-2013) and calibration (2013-2015) of total weekly ET. The red solid line represents the weekly observed ET. The black dashed line represents the baseline ET runs. The blue shaded areas represent the 30 best realizations based on ET from flux towers for calibration. The green shaded region represents the calibration period and yellow shaded represents the validation period.

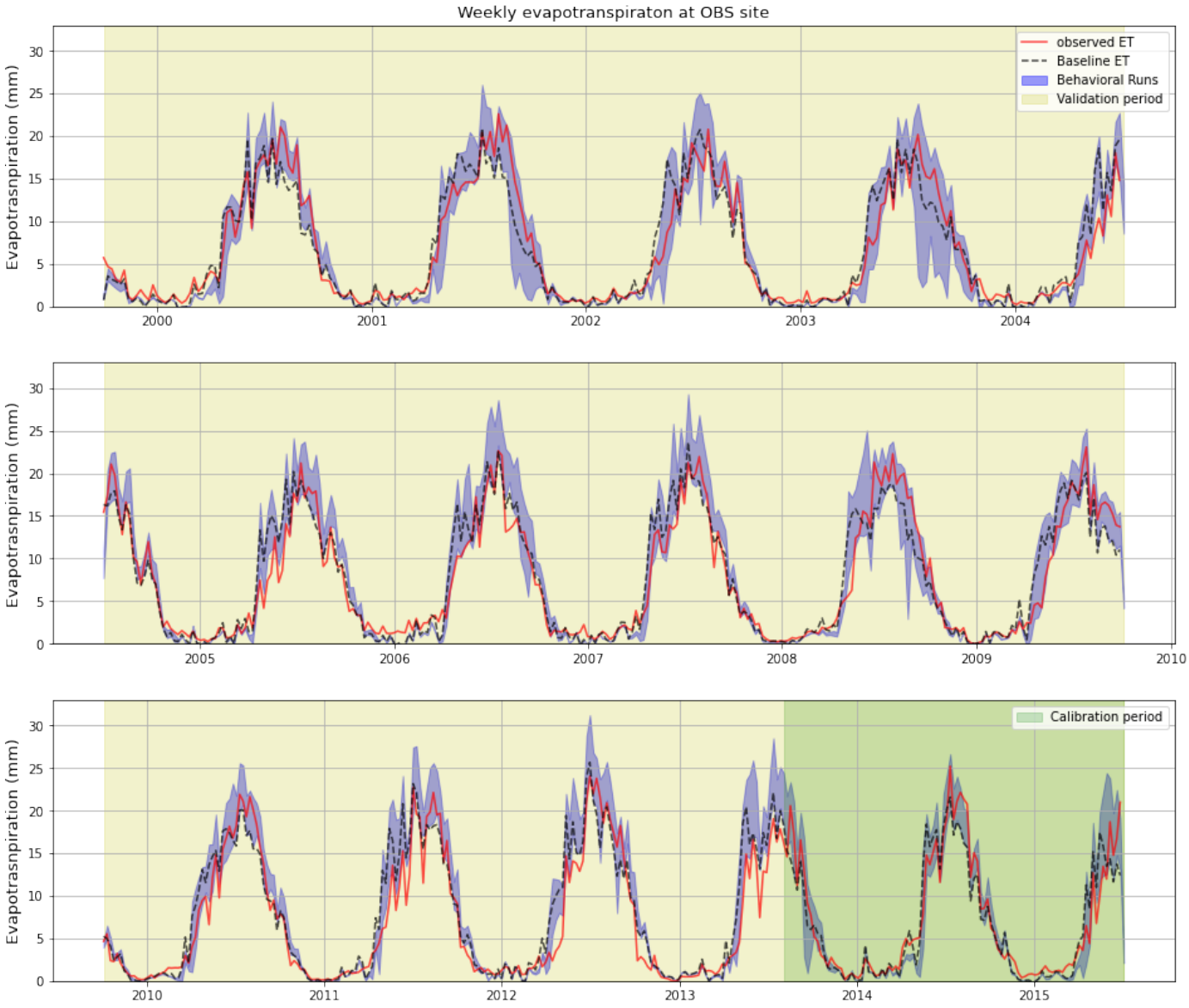

Figure 12: OBS model validation (1999-2013) and calibration (2013-2015) of total weekly ET. The red solid line represents the weekly observed ET. The black dashed line represents the baseline ET runs. The blue shaded areas represent the 30 best realizations based on ET from flux towers for calibration. The green shaded region represents the calibration period and yellow shaded represents the validation period.

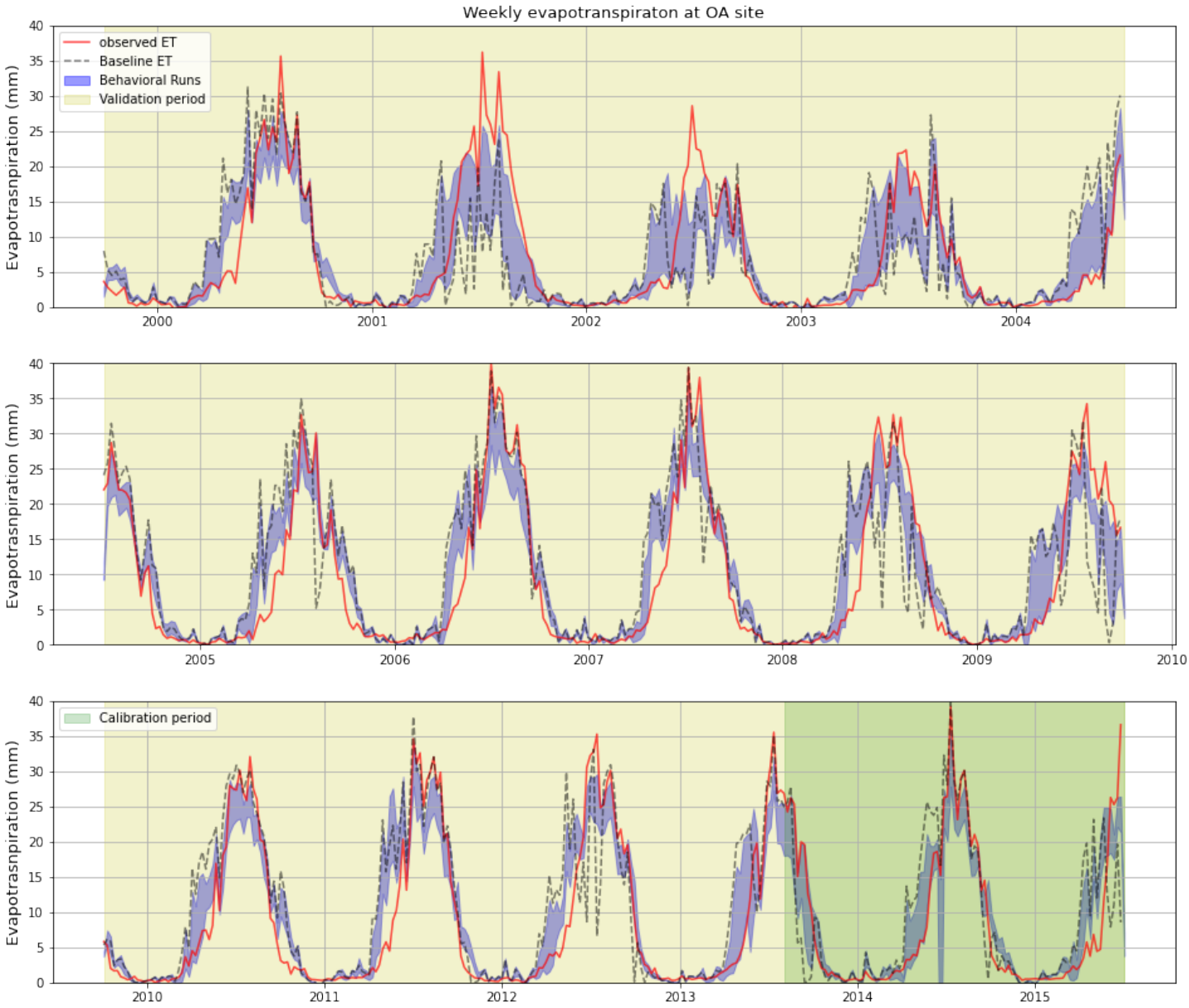

Figure 13: OA model validation (1999-2013) and calibration (2013-2015) of total weekly ET. The red solid line represents the weekly observed ET. The black dashed line represents the baseline ET runs. The blue shaded areas represent the 30 best realizations based on ET from flux towers for calibration. The green shaded region represents the calibration period and yellow shaded represents the validation period.

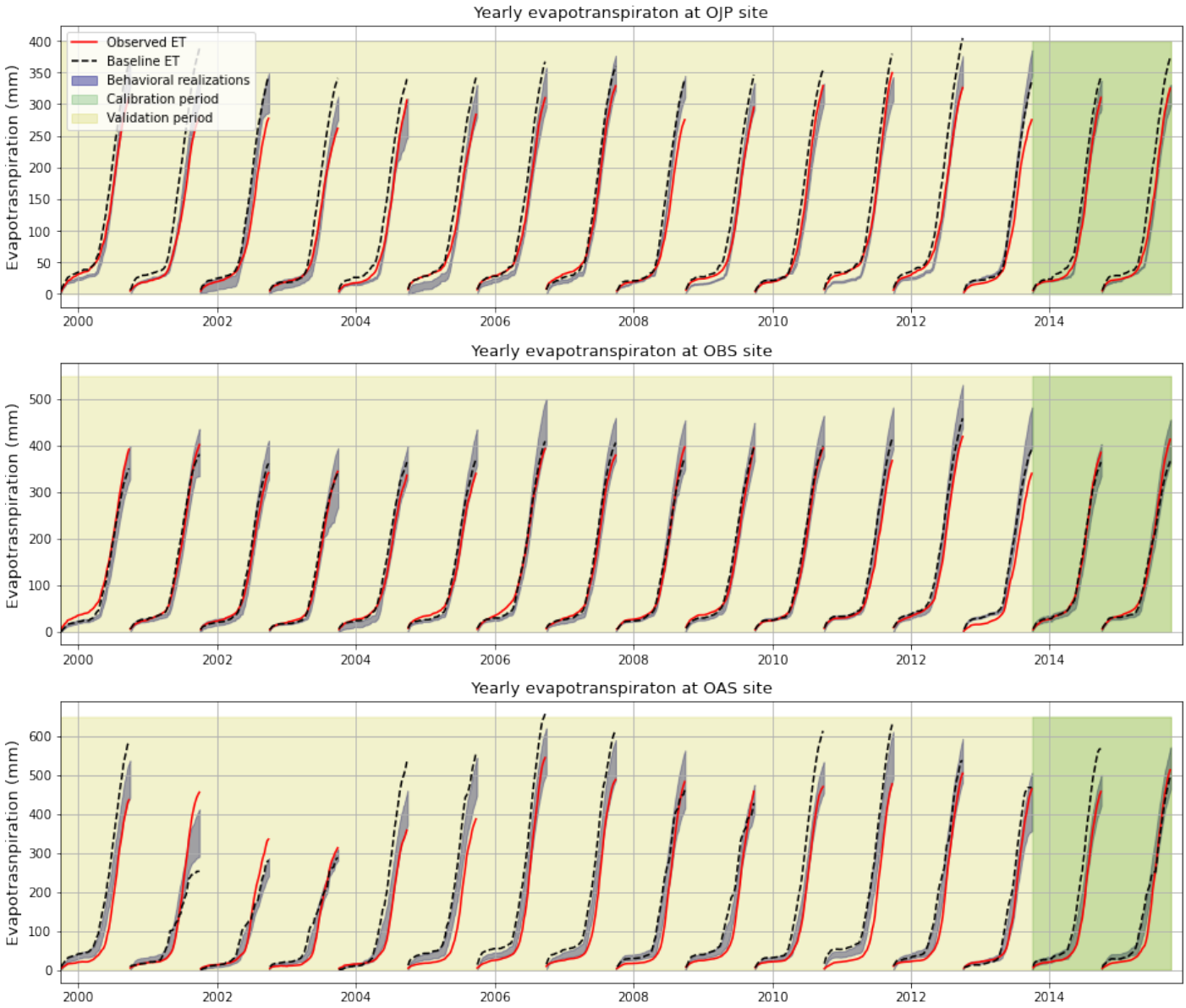

Figure 14: OJP, OBS and OA model validation (1999-2013) and calibration (2013-2015) of annual ET. The black dashed line represents the baseline ET runs. The red solid line represents the annual observed ET. The blue shaded areas represent the 30 best realizations after using observed ET for calibration. The green shaded region represents the calibration period and yellow shaded represents the validation period.

Table 9: Median of the total uncertainty of the ET, Infiltration, Drainage and Runoff when ET is used as a constrain

Sites	ET (mm/yr)	Infiltration (mm/yr)	Drainage (mm/yr)	Runoff (mm/yr)
OJP	41	91	101	80
OBS	89	134	111	125
OA	100	88	43	78

At OBS, we see the largest uncertainties in infiltration, drainage and runoff. OA, on the other hand, has the highest uncertainty in ET and the lowest uncertainty in the other fluxes, particularly in the drainage flux. Uncertainty of ET is the lowest at OJP. Although the uncertainty range seems to be different for different sites, we still see a large uncertainty in the fluxes at all sites. The improved performance at simulating ET did not adequately constrain the other fluxes. However, it is important to note that the model was configured to run by assigning the hydraulic properties directly rather than using the pedotransfer function. The uncertainty analysis revealed parameter equifinality which means there is no single best model parameter set and that a set of parameters can generate similar calibrated results. Ireson et al. (2021) showed that a hydraulic-properties-based configuration gives parameters more degree of freedom and as a result has less constraint on fluxes compared to pedotransfer function. As a result, this brings in more uncertainty in the model fluxes. Performing calibration using only ET observations adjusts model simulation towards a better ET output and therefore, it may not therefore, may not guarantee a better simulation of other fluxes or states. Multi-Objective calibration tries to find the subset of behavioural simulations that work well for both.

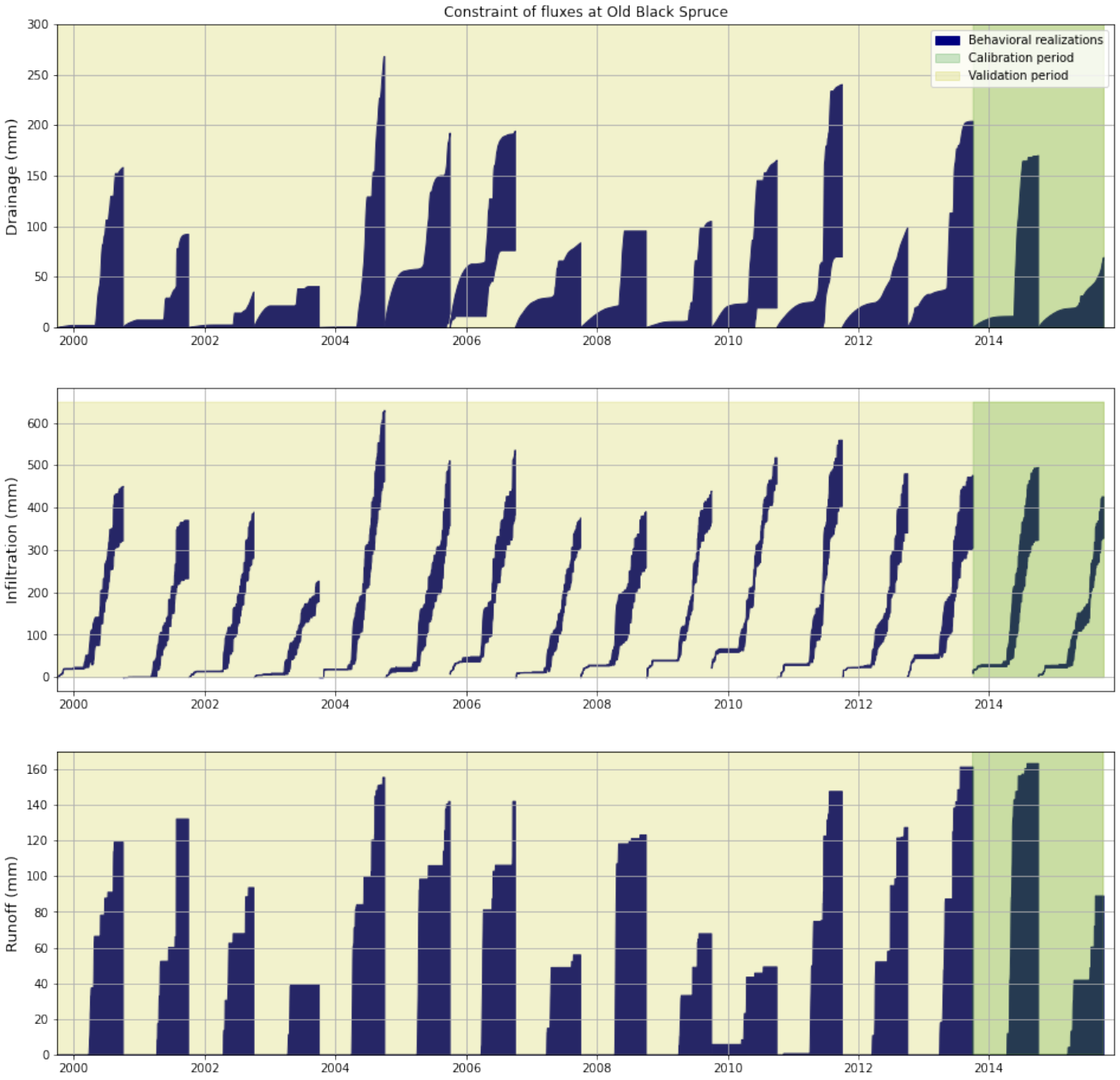

Figure 15: Constraint on fluxes (drainage, Infiltration and runoff) of the 30 best realization using ET from flux towers for calibration at OBS. The green shaded region represents the validation period (1999-2013) and yellow shaded represents the calibration period.

A multi-objective calibration represents multiple aspects of hydrological behavior as it in incorporates more information from the data sources. At OBS and OAS, model performance improves in terms of cumulative change in storage over the soil profile in the multi-objective calibration (Figure 16). At OJP, the constraint on the cumulative change in storage over the soil profile did improve but the observed values did not fall in the uncertainty bounds. The cumulative change in storage over the profile at all sites manages to capture the overall change in the seasonal pattern, but there is a slower rise of simulated than observed total liquid water content during the spring.

A surprising result was that including the soil moisture in the calibration as part of the multi-objective function did not necessarily improve the constrain on other fluxes (Table 10) at OJP, OBS and OA. Table 10 summarizes the constraint on the modeled fluxes at all three sites using single objective and multi objective calibration by taking the mean of the total uncertainty over the calibration period. Increased uncertainty in ET is expected but they are huge in OJP and OBS.

Table 10: Mean of the total uncertainty of the ET, Infiltration, drainage and runoff using single and multi-objective calibration during the calibration period.

	ET/mm		Runoff/mm		Drainage/mm		Infiltration/mm	
Objective Function	Single	Multiple	Single	Multiple	Single	Multiple	Single	Multiple
OJP	30	61	94	104	122	151	100	108
OBS	65	163	124	76	120	120	132	77
OAS	199	213	62	64	46	76	89	108

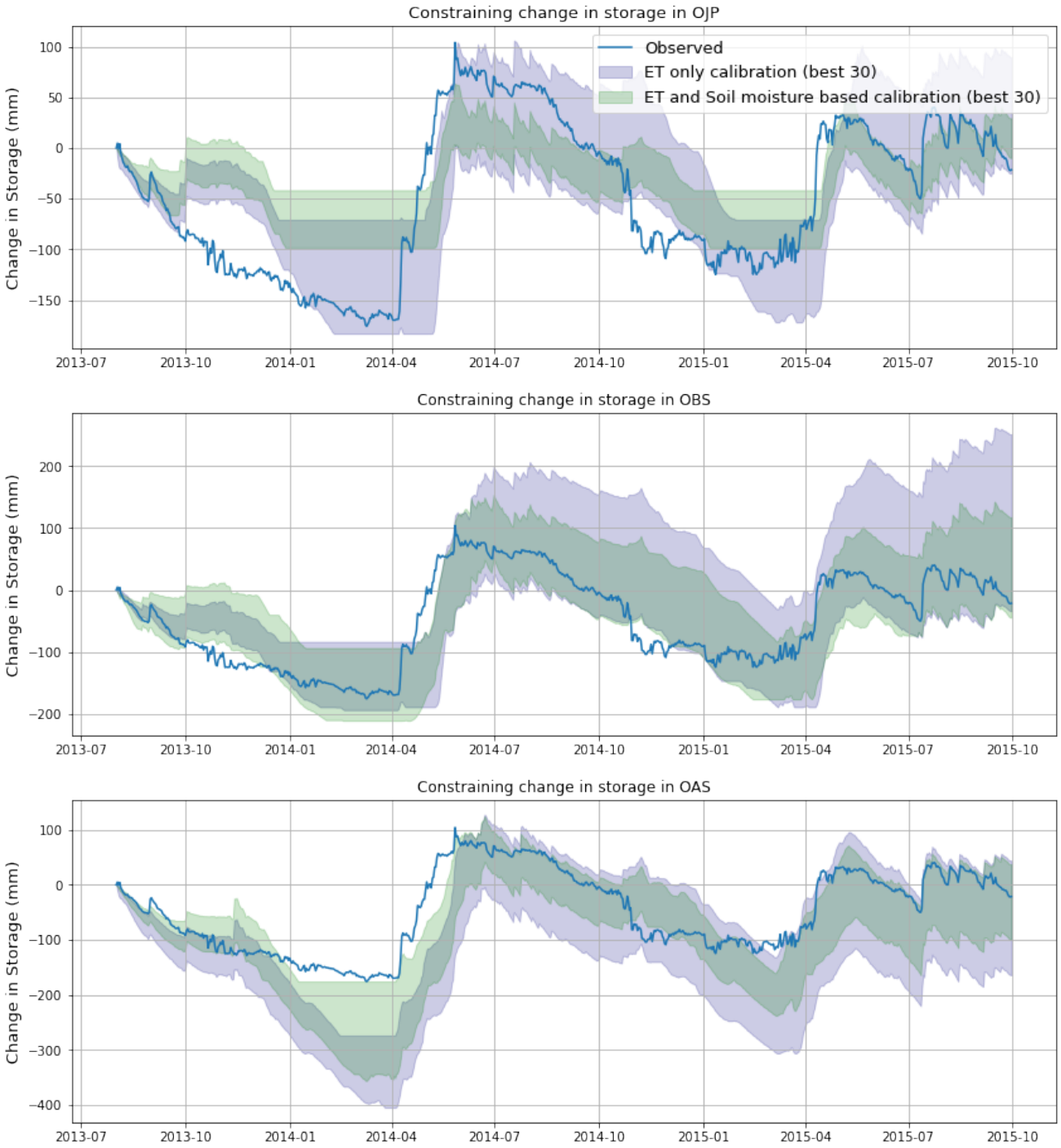

Figure 16: Comparison of single-objective (ET only) and multi-objective (ET and soil moisture) constraints on the seasonal cycles of soil water storage for two years in the calibration period (shaded areas). The uncertainty bounds show the range of the 30 best realizations from a Monte-Carlo process. The blue line shows the observed values.

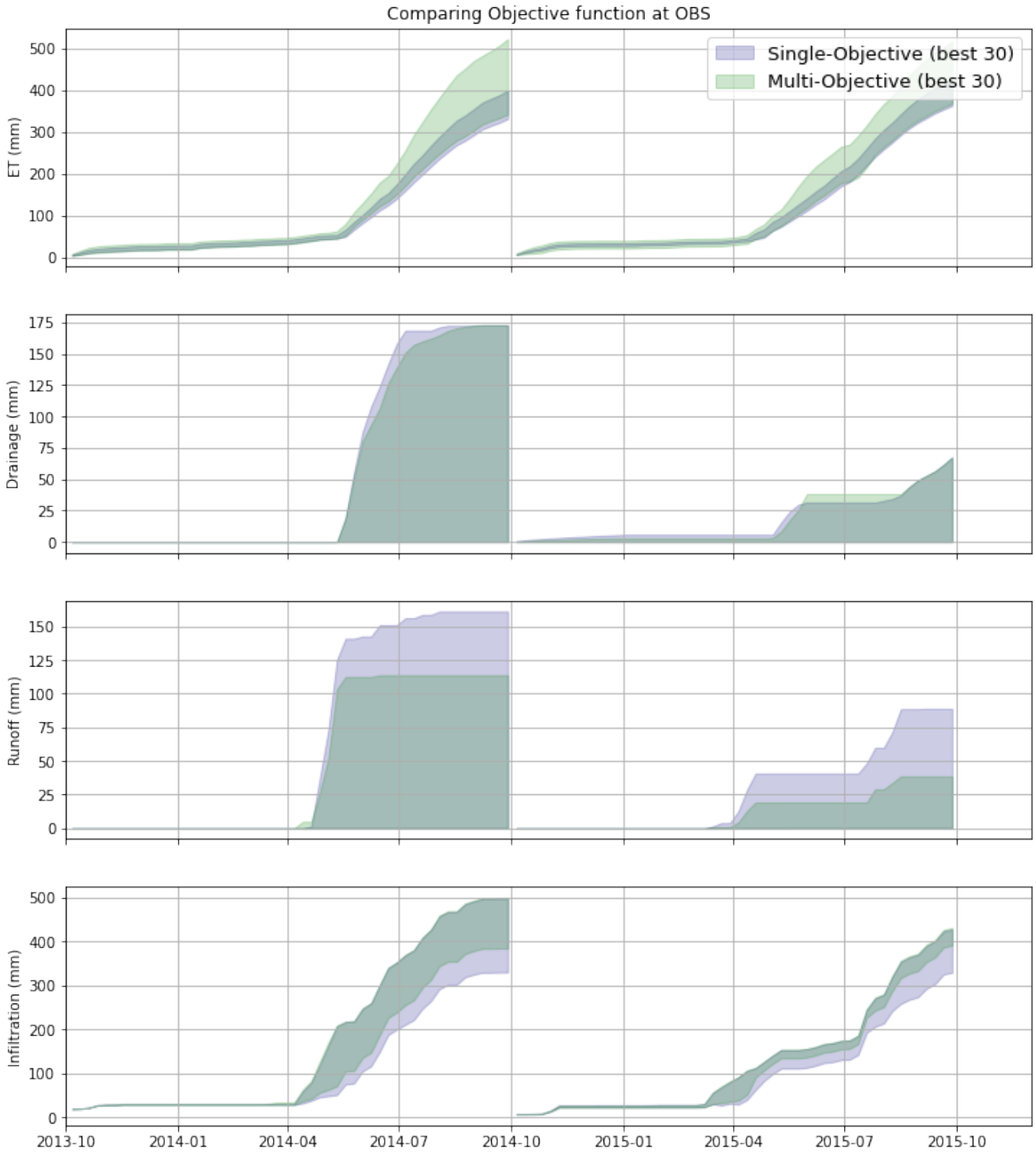

Figure 17: Comparison of single-objective (ET only) and multi-objective (ET and soil moisture) constraints on the seasonal cycles of ET, drainage, runoff and infiltration for two years in the calibration period (shaded areas). The uncertainty bounds show the range of the 30 best realizations from a Monte-Carlo process.

At OBS, adoption of a multi-objective function decreased the uncertainty bounds for runoff and infiltration, while drainage was unchanged. We see an increase in uncertainty bounds at OJP and OBS. Overall, the uncertainty bounds are not consistently reduced when we constrain the fluxes using multi-objective calibration. Other studies have noted that the use of multi-objective functions can reduce uncertainty and equifinality by adding constraints (Wagener and Gupta 2005; Tang et al., 2006; Reed et al., 2013).

$$\frac{dS}{dt} = I - ET - D \tag{35}$$

where $\frac{dS}{dt}$ is the change in storage, I is the infiltration, D is the drainage

Bringing soil moisture and ET in the equation, like we did in the multi-objective calibration, does bring in more known quantities in the equation but we still have two unknowns: infiltration and drainage. Overestimation of one flux can still be compensated by underestimation of another flux. Overall, calibration did bring some improvement on the ET performance of the model, but even with multi objective calibration (ET and soil moisture) we still have a significant problem with equifinality, and hence uncertainty in the modelled fluxes. Uncertainty and equifinality are inevitable in modeling until we have sufficient information about the parameters to completely constrain the parameter range. Calibration of the model did not result to satisfactory solution, and it shows there are limitations in the model structure. To improve the model results, we will need better descriptions of transpiration in the algorithms and parametrizations.

6 Conclusion

Previous studies have shown land surface models have overestimated ET in the Southern Boreal Plains Ecozone. We also showed that the baseline configuration of CLASS overestimated ET at the BERMS OJP, OBS and OA sites during the melt period. An investigation of the model found some potential limitations with the way that transpiration is represented during the spring melt period, which may be responsible for this systematic error. There is no representation of freezing point depression in the model, meaning that when the soil thaws, it remains at 0 ℃ for an extended period. Transpiration begins in the model as soon as there is enough thawed liquid water, and hence a significant amount of transpiration happens during the thaw period while the soils are at 0 ℃. In reality, due to freezing point depression, thawing takes place below 0 ℃, and when the soil reaches 0 ℃ it should be ice free. We speculate that no transpiration should take place below 0 ℃, since the plant should not be able to extract and transport super-cooled water. Therefore, we hypothesize that no transpiration should take place while there is ice in the pore-space. We found that if we subtract the transpiration that took place during thaw, when simulated soil temperature is 0 ℃ and ice was present, from the total ET, the resulting ET was more consistent with the flux tower observations. We therefore recommend two modifications to CLASS that we think would improve spring ET: 1) a freezing point depression should be implemented in the model, by including a soil freezing characteristic curve; 2) the water stress function should be modified to shut down transpiration when the soil temperature is less than or equal to 0 ℃. There are number of potential limitations in the model. The root system in CLASS is not dynamic, however, in real world, roots die in winter and regrow in spring before transpiration begins. A dynamic root system could potentially improve the transpiration during the spring season. Improved understanding of tree physiology and a direct field study during the winter and spring may provide useful insights

and directions. While the findings of this research demonstrated the important role of transpiration in offsetting the overestimation of ET in the model, it is important to note that other factors such as soil evaporation (Sun and Verseghy, 2019; Meyer et al., 2021) and intercepted water may also account for the different between simulated and observed ET. Our results also demonstrated that calibration using ET from flux tower estimates did improve the ET performance during the melt period, albeit with large uncertainty bounds of the other hydrological fluxes. Multi-objective calibration, including soil moisture along with flux tower ET estimates, did not improve the constraint on simulated infiltration and drainage. This works suggests a need for a direct field study of hydraulic parameters associated with infiltration and drainage to better constrain the model uncertainties.

References

Amankwah, S. K., Ireson, A., Maule, C., Brannen, R., & Mathias, S. A. (2021, April 5). Quantifying the soil freezing characteristic: The dominant role of salt exclusion (world) [Preprint]. Earth and Space Science Open Archive; Earth and Space Science Open Archive. https://doi.org/10.1002/essoar.10506652.1

Appels, W. M., Coles, A. E., & McDonnell, J. J. (2018). Infiltration into frozen soil: From core-scale dynamics to hillslope-scale connectivity. Hydrological Processes, 32(1), 66–79. https://doi.org/10.1002/hyp.11399

Barr, A. G., Morgenstern, K., Black, T. A., McCaughey, J. H., & Nesic, Z. (2006). Surface energy balance closure by the eddy-covariance method above three boreal forest stands and implications for the measurement of the CO2 flux. Agricultural and Forest Meteorology, 140(1), 322–337. https://doi.org/10.1016/j.agrformet.2006.08.007

Barr, A. G., van der Kamp, G., Black, T. A., McCaughey, J. H., & Nesic, Z. (2012). Energy balance closure at the BERMS flux towers in relation to the water balance of the White Gull Creek watershed 1999–2009. Agricultural and Forest Meteorology, 153, 3–13. https://doi.org/10.1016/j.agrformet.2011.05.017

Bartlett, P. A., Harry McCaughey, J., Lafleur, P. M., & Verseghy, D. L. (2003). Modelling evapotranspiration at three boreal forest stands using the CLASS: Tests of parameterizations for canopy conductance and soil evaporation. International Journal of Climatology, 23(4), 427–451. https://doi.org/10.1002/joc.884

Bodhinayake, W., & Si, B. C. (2004). Near-saturated surface soil hydraulic properties under different land uses in the St Denis National Wildlife Area, Saskatchewan, Canada. Hydrological Processes, 18(15), 2835–2850. https://doi.org/10.1002/hyp.1497

Cavanaugh, M. L., Kurc, S. A., & Scott, R. L. (2011). Evapotranspiration partitioning in semiarid shrubland ecosystems: A two-site evaluation of soil moisture control on transpiration. Ecohydrology, 4(5), 671–681. https://doi.org/10.1002/eco.157

Chen, J. M., & Black, T. A. (1992). Defining leaf area index for non-flat leaves. Plant, Cell & Environment, 15(4), 421–429. https://doi.org/10.1111/j.1365-3040.1992.tb00992.x

Chen, L., Li, Y., Chen, F., Barr, A., Barlage, M., & Wan, B. (2016). The incorporation of an organic soil layer in the Noah-MP land surface modeland its evaluation over a boreal aspen forest. Atmospheric Chemistry and Physics, 16(13), 8375–8387. https://doi.org/10.5194/acp-16-8375-2016

Chen, X., Liang, X., Xia, J., & She, D. (2018). Impact of Lower Boundary Condition of Richards' Equation on Water, Energy, and Soil Carbon Based on Coupling Land Surface and Biogeochemical Models. Pedosphere, 28(3), 497–510. https://doi.org/10.1016/S1002-0160(17)60371-0

Cherkauer, K. A., & Lettenmaier, D. P. (2003). Simulation of spatial variability in snow and frozen soil. Journal of Geophysical Research: Atmospheres, 108(D22). https://doi.org/10.1029/2003JD003575

Crow, W. T., Wood, E. F., & Pan, M. (2003). Multiobjective calibration of land surface model evapotranspiration predictions using streamflow observations and spaceborne surface radiometric temperature retrievals. Journal of Geophysical Research: Atmospheres. http://handle.nal.usda.gov/10113/59897

Damour, G., Simonneau, T., Cochard, H., & Urban, L. (2010). An overview of models of stomatal conductance at the leaf level. Plant, Cell & Environment, 33(9), 1419–1438. https://doi.org/10.1111/j.1365-3040.2010.02181.x

Ding, R., Kang, S., Du, T., Hao, X., & Zhang, Y. (2014). Scaling up stomatal conductance from leaf to canopy using a dual-leaf model for estimating crop evapotranspiration. PloS One, 9(4), e95584. https://doi.org/10.1371/journal.pone.0095584

Garrote, L., & Bras, R. L. (1995). A distributed model for real-time flood forecasting using digital elevation models. Journal of Hydrology, 167(1), 279–306. https://doi.org/10.1016/0022-1694(94)02592-Y

Gerosa, G., Mereu, S., Finco, A., & Marzuoli, R. (2012). Stomatal Conductance Modeling to Estimate the Evapotranspiration of Natural and Agricultural Ecosystems. https://doi.org/10.5772/21825

He, H., Dyck, M., Zhao, Y., Si, B., Jin, H., Zhang, T., Lv, J., & Wang, J. (2016). Evaluation of five composite dielectric mixing models for understanding relationships between effective permittivity and unfrozen water content. Cold Regions Science and Technology, 130, 33–42. https://doi.org/10.1016/j.coldregions.2016.07.006

Houska, T., Multsch, S., Kraft, P., Frede, H.-G., & Breuer, L. (2013). Monte Carlo-Based Calibration and Uncertainty Analysis of a Coupled Plant Growth and Hydrological Model. Biogeosciences Discussions, 10, 19509–19540. https://doi.org/10.5194/bgd-10-19509-2013

Ireson, A., Amankwah, S., Basnet, S., Bobenic, T., Braaten, M., Brannen, R., Brauner, H., Elrashidy, M., Sanchez-Rodriguez, I., & Barr, A. (2021). Using observed soil moisture to constrain the uncertainty of simulated hydrological fluxes. Authorea Preprints.

Ireson, A. M., van der Kamp, G., Ferguson, G., Nachshon, U., & Wheater, H. S. (2013). Hydrogeological processes in seasonally frozen northern latitudes: Understanding, gaps and challenges. Hydrogeology Journal, 21(1), 53–66. https://doi.org/10.1007/s10040-012-0916-5

Jagtar Bhatti, V. B., Mark Castonguay, R. E., & Arp, P. A. (2006). Modeling snowpack and soil temperature and moisture conditions in a jack pine, black spruce and aspen forest stand in central Saskatchewan (BOREAS SSA). Canadian Journal of Soil Science, 86(Special Issue), 203–217. https://doi.org/10.4141/S05-088

Jarvis, P. G. (1976). The Interpretation of the Variations in Leaf Water Potential and Stomatal Conductance Found in Canopies in the Field. Philosophical Transactions of the Royal Society of London Series B, 273, 593–610. https://doi.org/10.1098/rstb.1976.0035

Jarvis—2011—Simple physics-based models of compensatory plant .pdf. (n.d.). Retrieved October 28, 2019, from https://www.hydrol-earth-syst-sci.net/15/3431/2011/hess-15-3431-2011.pdf

Mellander, P.-E., Bishop, K., & Lundmark, T. (2004). The influence of soil temperature on transpiration: A plot scale manipulation in a young Scots pine stand. Forest Ecology and Management, 195, 15–28. https://doi.org/10.1016/j.foreco.2004.02.051

Mellander, P.-E., Stähli, M., Gustafsson, D., & Bishop, K. (2006). Modelling the effect of low soil temperatures on transpiration by Scots pine. Hydrological Processes, 20, 1929–1944. https://doi.org/10.1002/hyp.6045

Meyer, G., Humphreys, E. R., Melton, J. R., Cannon, A. J., & Lafleur, P. M. (2021). Simulating shrubs and their energy and carbon dioxide fluxes in Canada's Low Arctic with the Canadian Land Surface Scheme Including Biogeochemical Cycles (CLASSIC). Biogeosciences, 18(11), 3263–3283. https://doi.org/10.5194/bg-18-3263-2021

Mohammed, A. A., Kurylyk, B. L., Cey, E. E., & Hayashi, M. (2018). Snowmelt Infiltration and Macropore Flow in Frozen Soils: Overview, Knowledge Gaps, and a Conceptual Framework. Vadose Zone Journal, 17(1), 180084. https://doi.org/10.2136/vzj2018.04.0084

Nazarbakhsh, M., Ireson, A. M., & Barr, A. G. (2020). Controls on evapotranspiration from jack pine forests in the Boreal Plains Ecozone. Hydrological Processes, 34(4), 927–940. https://doi.org/10.1002/hyp.13674

Scherler, M., Hauck, C., Hoelzle, M., Stähli, M., & Völksch, I. (2010). Meltwater infiltration into the frozen active layer at an alpine permafrost site. Permafrost and Periglacial Processes, 21(4), 325–334. https://doi.org/10.1002/ppp.694

Scott, R. L., Huxman, T. E., Cable, W. L., & Emmerich, W. E. (2006). Partitioning of evapotranspiration and its relation to carbon dioxide exchange in a Chihuahuan Desert shrubland. Hydrological Processes, 20(15), 3227–3243. https://doi.org/10.1002/hyp.6329

Stadler, D., Sta¨hli, M., Aeby, P., & Flu¨hler, H. (2000). Dye Tracing and Image Analysis for Quantifying Water Infiltration into Frozen Soils. Soil Science Society of America Journal, 64(2), 505–516. https://doi.org/10.2136/sssaj2000.642505x

Stähli, M., Jansson, P.-E., & Lundin, L.-C. (1996). Preferential Water Flow in a Frozen Soil—A Two-Domain Model Approach. Hydrological Processes, 10(10), 1305–1316. https://doi.org/10.1002/(SICI)1099-1085(199610)10:10<1305::AID-HYP462>3.0.CO;2-F

Stähli, M., Jansson, P.-E., & Lundin, L.-C. (1999). Soil moisture redistribution and infiltration in frozen sandy soils. Water Resources Research, 35(1), 95–103. https://doi.org/10.1029/1998WR900045

Ukkola, A. M., Kauwe, M. G. D., Pitman, A. J., Best, M. J., Abramowitz, G., Haverd, V., Decker, M., & Haughton, N. (2016). Land surface models systematically overestimate the intensity, duration and magnitude of seasonal-scale evaporative droughts. Environmental Research Letters, 11(10), 104012. https://doi.org/10.1088/1748-9326/11/10/104012

Vrugt, J., ter Braak, C., Gupta, H., & Robinson, B. (2008). Equifinality of Formal (DREAM) and Informal (GLUE) Bayesian Approaches in Hydrologic Modeling? Stochastic Environmental Research and Risk Assessment, 23, 1011–1026. https://doi.org/10.1007/s00477-008-0274-y

Watanabe, K., Kito, T., Dun, S., Wu, J. Q., Greer, R. C., & Flury, M. (2013). Water Infiltration into a Frozen Soil with Simultaneous Melting of the Frozen Layer. Vadose Zone Journal, 12(1). https://doi.org/10.2136/vzj2011.0188

Wu, C., & Chen, J. M. (2013). Deriving a new phenological indicator of interannual net carbon exchange in contrasting boreal deciduous and evergreen forests. Ecological Indicators, 24, 113–119. https://doi.org/10.1016/j.ecolind.2012.06.006

Wu, M., Jansson, P.-E., Wu, J., Tan, X., Wang, K., Chen, P., & Huang, J. (2018). Implementation of salt-induced freezing point depression function into CoupModel_v5 for improvement of modelling seasonally frozen soils. Hydrology and Earth System Sciences Discussions, 1–38. https://doi.org/10.5194/hess-2018-466

Wu, M., Zhao, Q., Jansson, P.-E., Wu, J., Tan, X., Duan, Z., Wang, K., Chen, P., Zheng, M., Huang, J., & Zhang, W. (2020). Improved soil hydrological modeling with the implementation of salt-induced freezing point depression in CoupModel: Model calibration and validation. Journal of Hydrology, 596. https://doi.org/10.1016/j.jhydrol.2020.125693

Zha, T., Barr, A. G., van der Kamp, G., Black, T. A., McCaughey, J. H., & Flanagan, L. B. (2010). Inter-annual variation of evapotranspiration from forest and grassland ecosystems in western canada in relation to drought. Agricultural and Forest Meteorology, 150(11), 1476–1484. https://doi.org/10.1016/j.agrformet.2010.08.003

Zhang, R., Liu, J., Gao, H., & Mao, G. (2018). Can multi-objective calibration of streamflow guarantee better hydrological model accuracy? Journal of Hydroinformatics, 20(3), 687–698. https://doi.org/10.2166/hydro.2018.131